AD-A065 561 PROTOTYPE DEVELOPMENT ASSOCIATES INC SANTA ANA CALIF F/G 13/5
APPLICATION OF NITINOL TO HIGH STIFFNESS STRUCTURAL JOINTS.(U)
FEB 79 R D BRUM, J C SCHUTZLER N60921-78-C-0049
UNCLASSIFIED PDA-TR-1390-00-01 NL

1 OF
AD
A065561

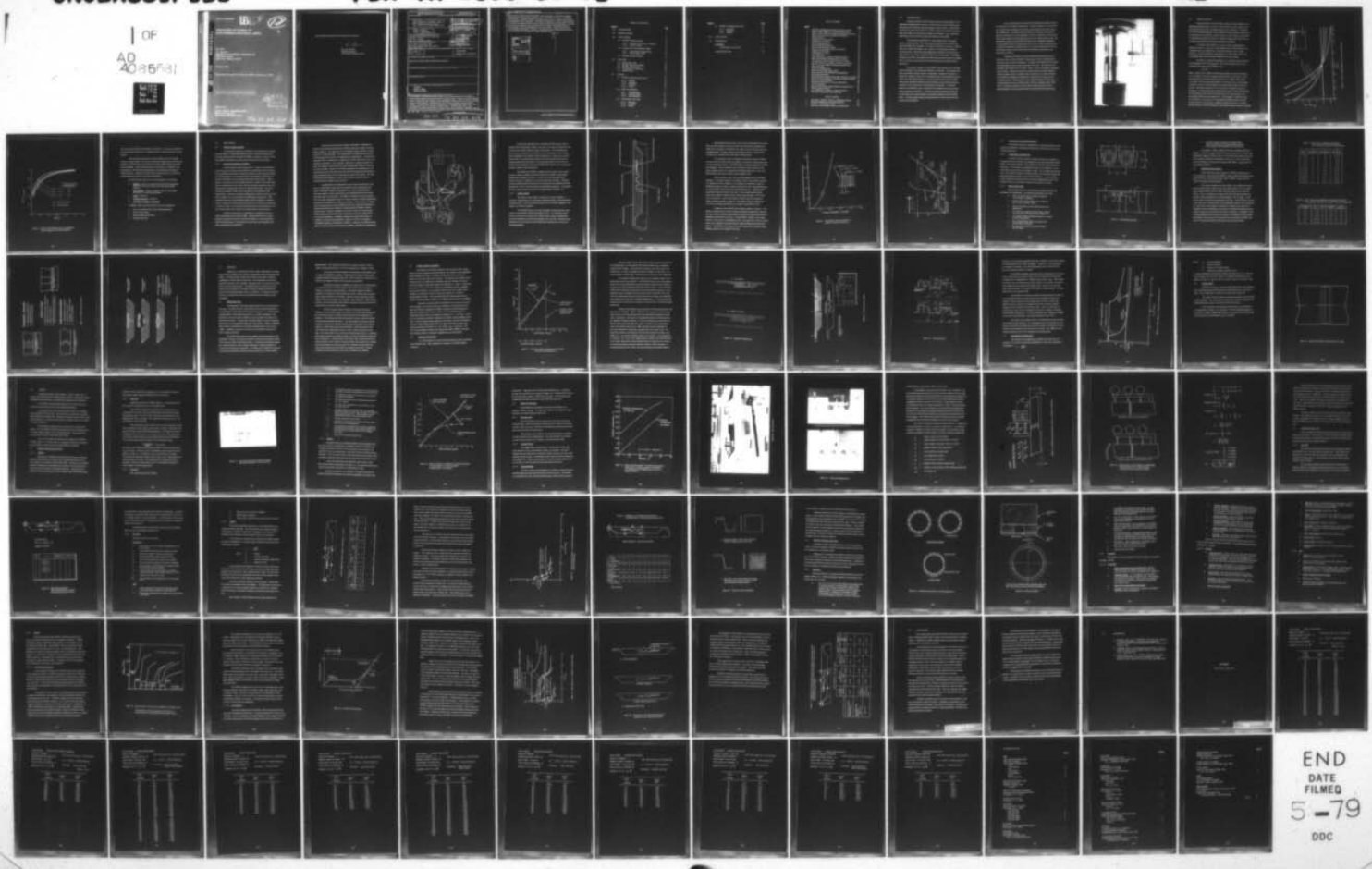

END
DATE FILMED
5-79
DDC

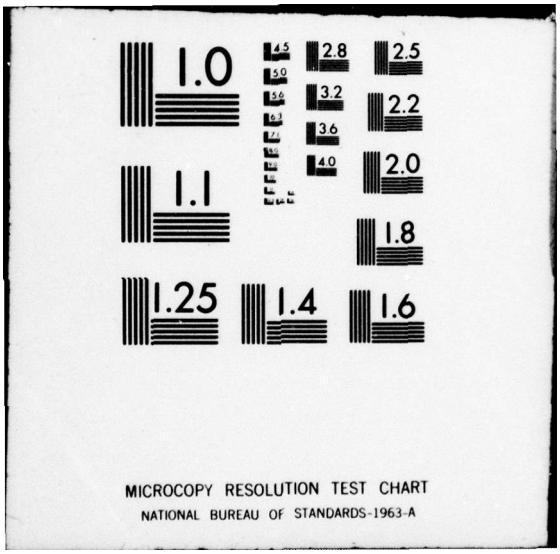
1.0
1.1
1.25
1.4
1.6
1.8
2.0
2.2
2.5
2.8
3.2
3.6
4.0
4.5
5.0
5.6
MICROCOPY RESOLUTION TEST CHART
NATIONAL BUREAU OF STANDARDS-1963-A

PDA TR 1390-00-01

LEVEL II

12

APPLICATION OF NITINOL TO HIGH STIFFNESS STRUCTURAL JOINTS

R.D. Brum
J.C. Schutzler
PROTOTYPE DEVELOPMENT ASSOCIATES, INC.
1740 Garry Avenue
Santa Ana, California 92705

February 1979

Final Report for period 20 February 1978 to 20 February 1979

Prepared for

NAVAL SURFACE WEAPONS CENTER
White Oak Laboratory
Silver Spring, Maryland 20910

This technical report has been reviewed and is approved.

DR. PAO HUANG
NITINOL Program
Naval Surface Weapons Center

UNCLASSIFIED

SECURITY CLASSIFICATION OF THIS PAGE (When Data Entered)

REPORT DOCUMENTATION PAGE

READ INSTRUCTIONS BEFORE COMPLETING FORM

1. REPORT NUMBER

2. GOVT ACCESSION NO.

3. RECIPIENT'S CATALOG NUMBER

4. TITLE (and Subtitle)

(6) Application of NITINOL to High Stiffness Structural Joints

(9) 5. TYPE OF REPORT & PERIOD COVERED
Final Report, 20 February 1978 – 20 February 1979

(14) 6. PERFORMING ORG. REPORT NUMBER
PDA-TR-1390-00-01

7. AUTHOR(s)

(10) R. D. Brum
J. C. Schutzler

(15) 8. CONTRACT OR GRANT NUMBER(s)
N60921-78-C-0045

9. PERFORMING ORGANIZATION NAME AND ADDRESS
Prototype Development Associates, Inc.
1740 Garry Avenue
Santa Ana, California 92705

(12) 10. PROGRAM ELEMENT, PROJECT, TASK AREA & WORK UNIT NUMBERS
62332N; F32392;
SF32392501; WA71

11. CONTROLLING OFFICE NAME AND ADDRESS
Naval Surface Weapons Center
White Oak, Silver Spring, MD 20910
Attn: Code CA-31

(11) 12. REPORT DATE
February 1979

13. NUMBER OF PAGES
97

14. MONITORING AGENCY NAME & ADDRESS (if different from Controlling Office)

(12) 94 pl

15. SECURITY CLASS. (of this report)
Unclassified

15a. DECLASSIFICATION DOWNGRADING SCHEDULE

16. DISTRIBUTION STATEMENT (of this Report)

Approved for public release; distribution unlimited.

17. DISTRIBUTION STATEMENT (of the abstract entered in Block 20, if different from Report)

18. SUPPLEMENTARY NOTES

19. KEY WORDS (Continue on reverse side if necessary and identify by block number)

NITINOL
Memory Alloys
Structural Joints

20. ABSTRACT (Continue on reverse side if necessary and identify by block number)

The feasibility of utilizing the unique shape-recovery characteristics of NITINOL to achieve high preloads in structural joints was demonstrated. High performance missile systems require the shell stiffness in the longitudinal bending mode to be above a critical value to prevent dynamic coupling between the structure and high frequency control systems. In cases where the natural frequency is a limiting design requirement, joint preload greatly affects the design structural weight. NITINOL alloy can be used effectively to preload threaded joints to higher levels than obtainable by applying torque.

→over

DD FORM 1 JAN 73 1473 EDITION OF 1 NOV 65 IS OBSOLETE

UNCLASSIFIED

SECURITY CLASSIFICATION OF THIS PAGE (When Data Entered)

Several joint concepts utilizing NITINOL were conceived. A NITINOL preloaded threaded joint was designed, analyzed, built, assembled and tested. A NITINOL alloy having a cryogenic transition temperature was used; its compressive recovery characteristics were measured. A method of modeling the recovery characteristics of NITINOL in a general finite-element analysis of the joint was developed. Preload level and joint stiffness were measured for the NITINOL preloaded joint and a conventional, torque preloaded joint of the same design. Results agreed closely with analytical predictions. NITINOL preloading produced significant performance improvements over conventional torque preloaded joints.

TABLE OF CONTENTS

Section			Page
1.0	INTRODUCTION		5
2.0	DESIGN CRITERIA		9
3.0	JOINT DESIGN		13
	3.1 NITINOL Design Approach		13
		3.1.1 Structural Properties of NITINOL	13
		3.1.2 Design Concept	16
	3.2 Comparison to Conventional Designs		21
		3.2.1 Conventional Threaded Joint	21
		3.2.2 Bolted Flange Joints	21
	3.3 Alternate Design Concepts		23
4.0	ANALYSES		27
	4.1 NIFDI Finite Code		27
	4.2 NITINOL Behavior Modeling		29
	4.3 Baseline Joint Iteration		29
	4.4 Conventional Threaded Joint		35
	4.5 Scaling Effects		37
5.0	TESTING		39
	5.1 NITINOL Characterization Tests		39
		5.1.1 Purpose	39
		5.1.2 Apparatus	40
		5.1.3 Procedure	40
		5.1.4 Results	42
	5.2 Joint Test Apparatus		44
		5.2.1 Joint Specimen	44
		5.2.2 Loading Fixture	44
		5.2.3 Instrumentation	44
	5.3 Conventional Joint Tests		52
		5.3.1 Apparatus	52
		5.3.2 Procedure	52
		5.3.3 Results	55

Section			Page
	5.4	NITINOL Preloaded Joint Tests	61
		5.4.1 Apparatus	61
		5.4.2 Procedure	64
		5.4.3 Results	67
6.0	CONCLUSIONS		77
7.0	REFERENCES		79
	APPENDIX		
	STRUCTURAL TEST DATA		81
	DISTRIBUTION LIST		93

LIST OF FIGURES

Figure		Page
1	NITINOL preloaded joint specimen used for testing.	7
2	Effect of joint stiffness on structural deformation.	10
3	Effect of joint stiffness on longitudinal natural frequency.	11
4	Stress-strain temperature history of NITINOL.	15
5	Design concept.	17
6	Time before recovery onset.	19
7	NITINOL stress history.	20
8	Bolted flange geometry.	22
9	Alternate design concepts.	25
10	Sleeve-clamp analysis results.	26
11	Recovery stress-strain curve for NITINOL.	30
12	Original threaded joint.	32
13	NIFDI analysis results.	33
14	API thread form.	34
15	Joint stiffness as a function of applied moment.	36
16	Eight-inch NITINOL preloaded joint (1/2 size).	38
17	Test apparatus used for tests of recovery stress.	41
18	Recovery stress as a function of unrecovered strain.	43
19	Effect of preload weight on transition temperature.	45
20	Joint test set-up.	46
21	Test joint loading fixture.	47
22	Method of measuring joint rotation.	49
23	Measurement of joint deflections longitudinally.	50
24	Strain gage placement.	53
25	Determination of preload torque and coefficient of friction.	56
26	Measured joint stiffness as a function of applied moment.	58
27	Sources of joint compliance.	60
28	Meridional strains due to moment application.	62
29	Carrier assembly.	63
30	Stress-strain curves, polycrystalline normalized NiTi.	68
31	NITINOL stress history.	70
32	Joint stiffness as a function of applied moment.	72
33	Movement of joint after first load cycle.	73

LIST OF TABLES

1	Bolt sizes, maximum numbers, obtainable preloads.	24
2	Bolt size and numbers, protrustion distance.	24
3	Summary of strain gage results.	59
4	Summary of strain gage results, preloaded joint.	75

1.0 INTRODUCTION

High performance missile systems require the shell stiffness in the longitudinal bending mode to be above a critical value to prevent dynamic coupling between the structure and high frequency control systems. Body field or manufacturing joints can produce low stiffness regions which effectively act as hinges and reduce the body natural frequency accordingly. Thus, successful joint designs must meet both strength and stiffness requirements.

The principal requirement for a high-stiffness joint is the application of a large preload. The preload must be greater than or equal to the largest bending stress expected. The ability of NITINOL to return to a memory shape after plastic deformation can be utilized to develop large preloads in structural joints. Successful design application of NITINOL will provide preloaded joints with minimum load-path offset from the body shell. This design advantage of NITINOL will minimize in-plane local moments (eccentric loading) and, as a result, provide joints with lower weight and less internal volume protrusion.

The primary objective of the NITINOL joint program was to provide proof of principle of the unique high-stiffness joint concept. The program had three main phases; design, analysis, and testing. During the first phase, a design and evaluation criteria were formulated based on the functional requirements of missile shell structures. It was determined that the joint preload level greatly affected the design structural weight in cases where the natural frequency of the missile was a limiting design requirement. A literature search was conducted in order to determine the pertinent recovery and mechanical properties of NITINOL. A NITINOL preloaded threaded joint concept was developed and evaluated against conventional threaded and bolted flange joints. Alternate design concepts utilizing NITINOL in both tension and compression were identified.

A four-inch diameter by 0.060-inch wall aluminum missile structure was selected as the baseline configuration. Detailed analyses were performed on a threaded joint preloaded with NITINOL and preloaded with torque only for that configuration. The finite element method was selected as the means of analysis; specifically the NIFDI (Nonlinear Analysis of Interfaces with Friction between Discontinuous Solids having Interference Fit) finite element code. One-dimensional, closed form analytical techniques were completely inadequate for joint analysis since the actual stress states were at least two-dimensional. A method of analytically modeling NITINOL's recovery characteristics in the NIFDI finite element code was developed and baseline joint geometry was iteratively arrived at.

During the test phase, material characterization tests were performed in order to verify NITINOL's compressive recovery characteristics since they were not found in literature. A model of the baseline joint was built and conventional torque preloaded; joint tests were run. The joint was then preloaded with NITINOL and re-tested. Figure 1 shows the NITINOL preloaded joint specimen. Quantities measured included preload, preloaded stiffness, moment causing preload exceedance (M_{pe}), and strains at various locations. The NITINOL preloaded joint exhibited a 17-fold increase in M_{pe} over the conventional joint. Results agreed closely with the analytical predictions. It was determined that for the baseline case, NITINOL preloaded joints would allow a 26 percent reduction in overall shell weight and retain the same natural frequency as the baseline missile with conventional threaded joints.

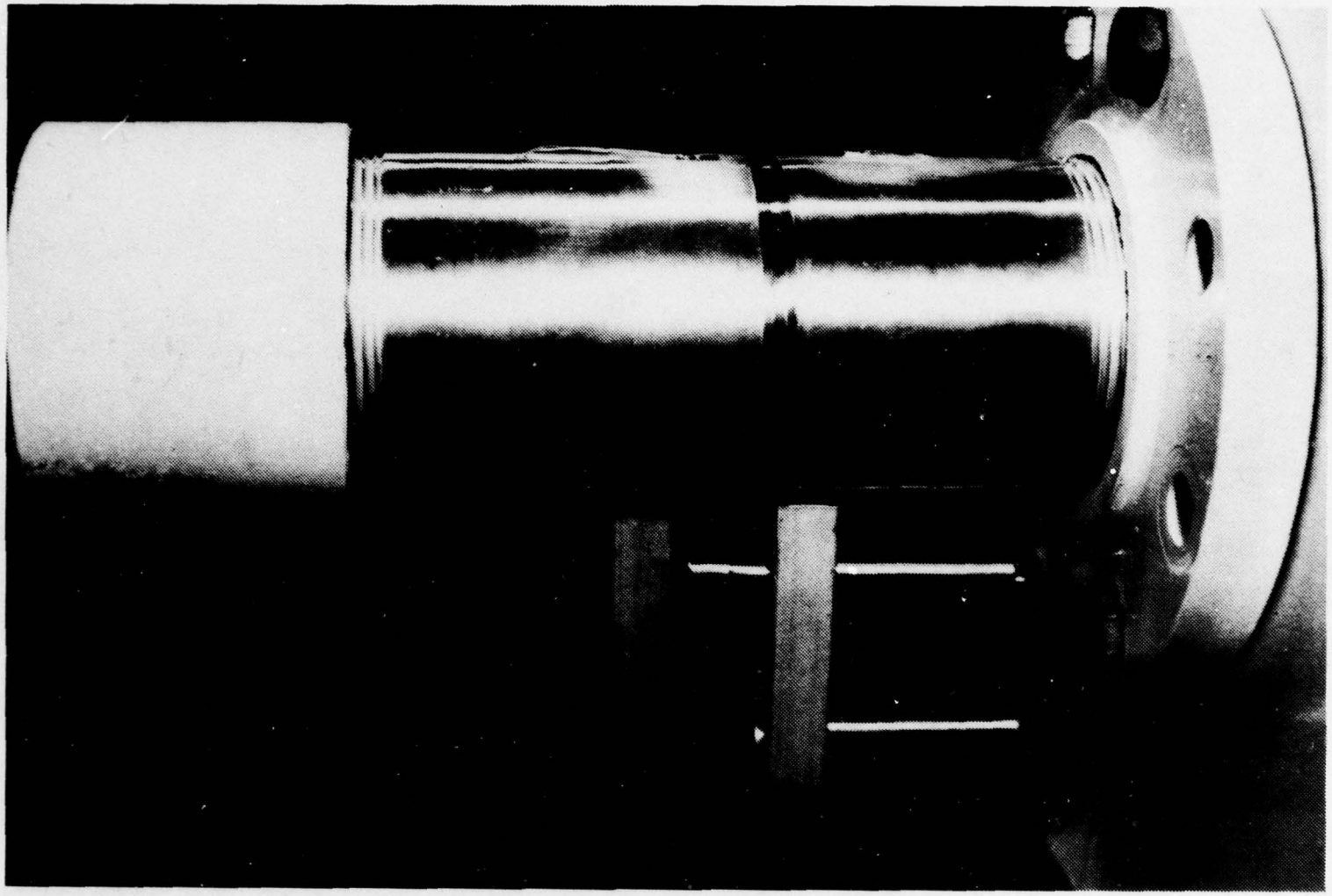

Figure 1. NITINOL preloaded joint specimen used for testing.

2.0 DESIGN CRITERIA

High performance missile systems require the shell stiffness in the longitudinal bending mode to be above a critical value to prevent dynamic coupling between the structure and high frequency control systems. In practice, the required bending stiffnesses can be achieved in body structures with the use of materials such as beryllium, graphite-epoxy or steel. However, body field or manufacturing joints can produce low stiffness regions which effectively act as hinges and reduce the body natural frequency accordingly.

The effect of joint stiffness on overall structural deformation is depicted in Figure 2. The ratio of joint stiffness (EI_j) to shell stiffness (EI_s) is plotted versus end deflection (δ), divided by deflection of the no-joint structure. It can be seen that as joint stiffness is reduced below that of the surrounding shell, overall structure deflections increase rapidly.

The effect of reduced joint stiffness on a vehicle's natural frequency in the longitudinal mode was examined. The natural frequency (ω_n) is proportional to the square root of stiffness (EI).

$$\omega_n \sim \sqrt{EI}$$

Figure 3 illustrates the effect of reduced joint stiffness on natural frequency. It is reasonably accurate for structures having three or more joints. It was calculated based on evenly distributed joints over the length of the vehicle. The modulus of the joint (E_j) and modulus of the structure (E_s) were specially averaged to obtain an overall modulus from which natural frequency was calculated. This approach becomes more accurate as the number of joints is increased. For the baseline case (4-inch diameter joint, 8-inch joint spacing), the joint stiffness after preload exceedance was only 40 percent that of the surrounding shell (reference Section 5.3). This produces a reduction in natural frequency of 14 percent over an equivalent preloaded missile structure. At first, that may not seem like a significant reduction; however, the same natural frequency could be obtained by utilizing high-stiffness joints and reducing

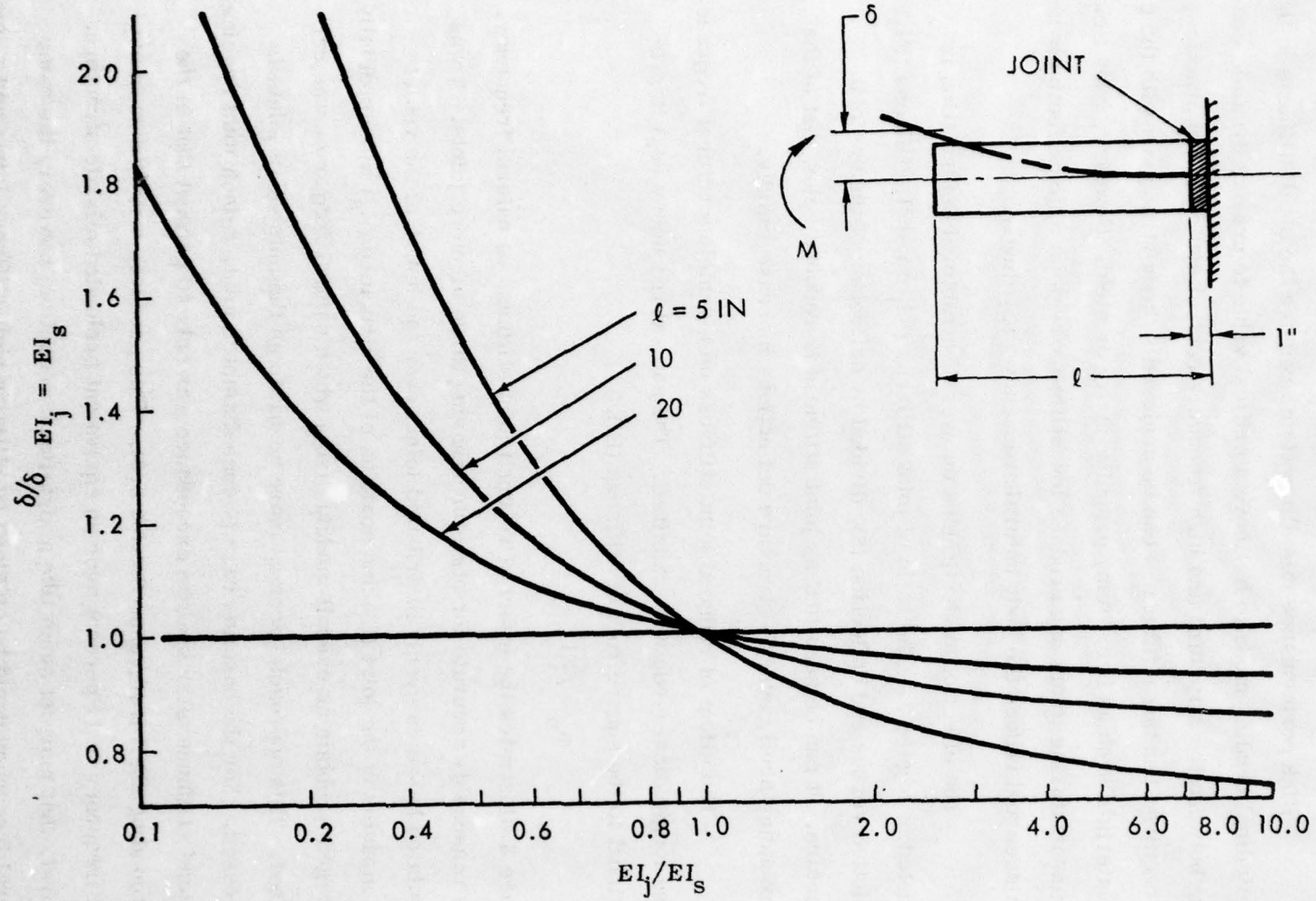

Figure 2. Effect of joint stiffness on structural deformation.

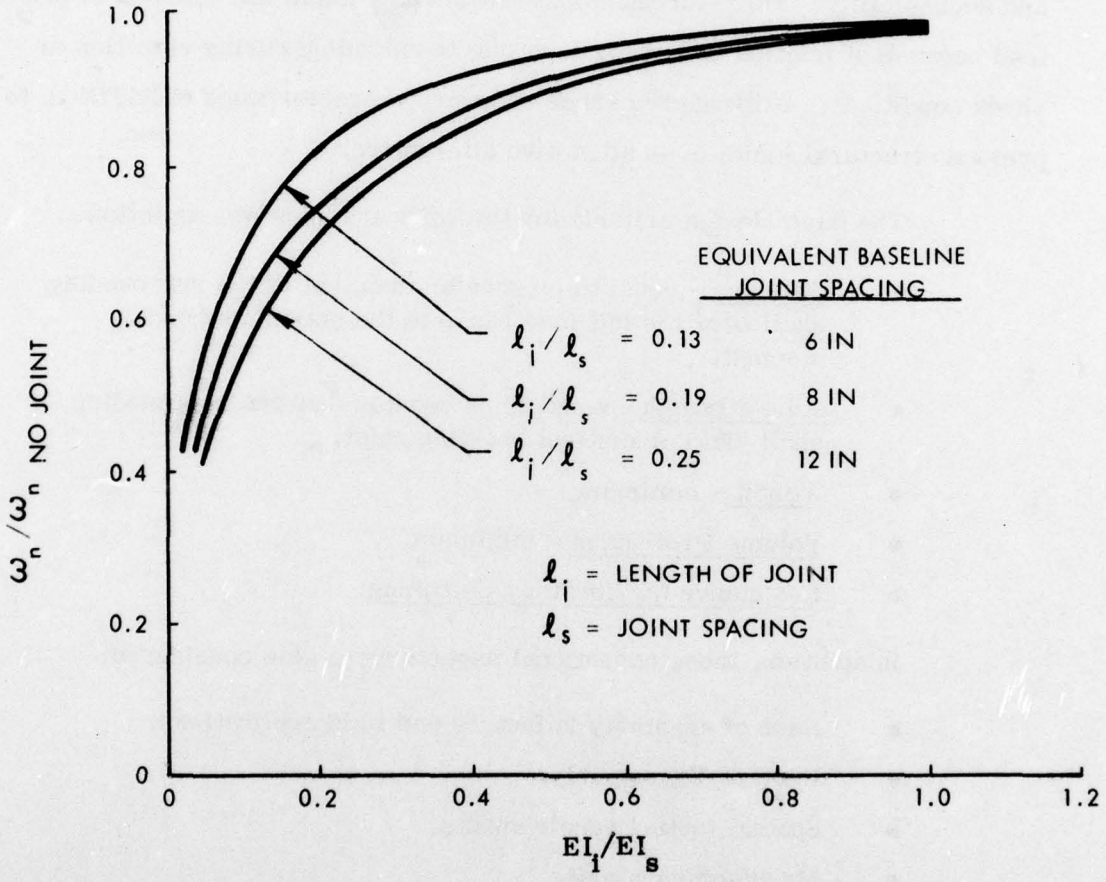

Figure 3. Effect of joint stiffness (EI_j) on longitudinal natural frequency of missile structure.

the overall shell thickness and weight by 26 percent. A 26 percent reduction in the overall shell weight can be a significant factor in high performance missile design.

The principal requirements for high-stiffness joints is the application of a large preload. This can be developed in flanged joints with threaded fasteners, but this type of joint generally has unacceptable volume protrusion and accessibility. Fully-threaded and breech-lock joints are difficult to preload because of friction and are susceptible to unloading during vibration or shock conditions. Utilizing the shape recovery characteristics of NITINOL to preload structural joints is an attractive alternative.

The basic design criteria for the joint analyses was as follows:

- Stiffness - equal to or greater than that of the surrounding shell over the full load range to the maximum bending moment.
- Joint Strength - equal to or greater than the surrounding shell yield or critical buckling point.
- Weight - minimum.
- Volume Protrusion - minimum.
- Resistance to Vibratory Unlocking.

In addition, these operational aspects were also considered:

- Ease of assembly in factory and field applications.
- Ease of disassembly.
- Special tooling requirements.
- Manufacturing cost.

3.0 JOINT DESIGN

3.1 NITINOL Design Approach

The structural properties of NITINOL were reviewed and a concept was developed for a unique high-stiffness joint for missile body structures. The joint concept utilizes the ability of NITINOL to return to a memory shape after plastic deformation to develop large preloads in structural joints.

3.1.1 Structural Properties of NITINOL

A brief literature search (References 1, 2 and 3) was conducted to review the memory recovery characteristics of 55-NITINOL and to compile a set of mechanical properties for design and analysis of joint preload concepts. For this application, it is desirable that the transformation temperature be below the minimum service operating temperature of the missile. This is because of the superior yield strength and elastic modulus in the transformed state as compared to the low values of these important properties in the martenistic state at temperatures below the transformation range. The transformation temperature range can be controlled by increasing the nickel concentration. However, the nickel concentration is limited to about 56.5 percent by weight due to the formation of an undesirable second phase. This restriction limits the transformation range to about 15 degrees F minimum. Further reductions in transformation temperature are achieved by substitution of cobalt for nickel. This enables the transformation to be depressed to cryogenic temperatures with no effect on the shape memory characteristics.

A NITINOL alloy shape is conditioned by annealing the material while constraining it in the desired shape. While annealing may be accomplished at temperatures between 750 and 1110 degrees F, it has been determined that 900 degrees F is an optimum memory heat treat temperature for many compositions of 55-NITINOL.

A stress-strain temperature history describing the intended use cycle for joint preload development by NITINOL segments is shown schematically in Figure 4. The segments will be machined to shape and then cooled by immersion in liquid nitrogen. The segment will be compressively deformed to about eight percent strain by loading between cooled platens. The deformed segments will be inserted into a threaded joint and the joint will be made up to contact the segments. As the segments' temperature approach ambient, the alloy will undergo transformation and will simultaneously attempt to expand to the memory shape. Because of constraint imposed by the threaded joint, the segments will exert force during recovery and will complete transformation at some equilibrium state of stress and strain as shown in the figure. The joint preload is then developed as a result of the NITINOL segments which are constrained from complete shape recovery.

Consideration of the intended use cycle reveals that the alloy must have a transformation range below the minimum service temperature and above a convenient cryogenic temperature (e.g., that of liquid nitrogen). With the exception of these requirements, the detailed behavior in the transformation range is unimportant. The ability of NITINOL to perform mechanical work while attempting to return to a memory shape is the basic engineering characteristic affecting the preloaded joint design. Measurements of mechanical work performed by several NITINOL alloys were reported in Reference 1. These measurements were taken for constant loads as functions of initial tensile strain. No data is available for recovery work from compressively deformed alloys with transformation temperatures in the low range desired for the joint application. Although no compressive stress-strain data are available, the elastic tensile modulus of about 12×10^6 psi is probably a reasonable estimate for preliminary evaluation. Likewise, an estimated yield stress of 80,000 psi from tensile tests is probably reasonable for compression.

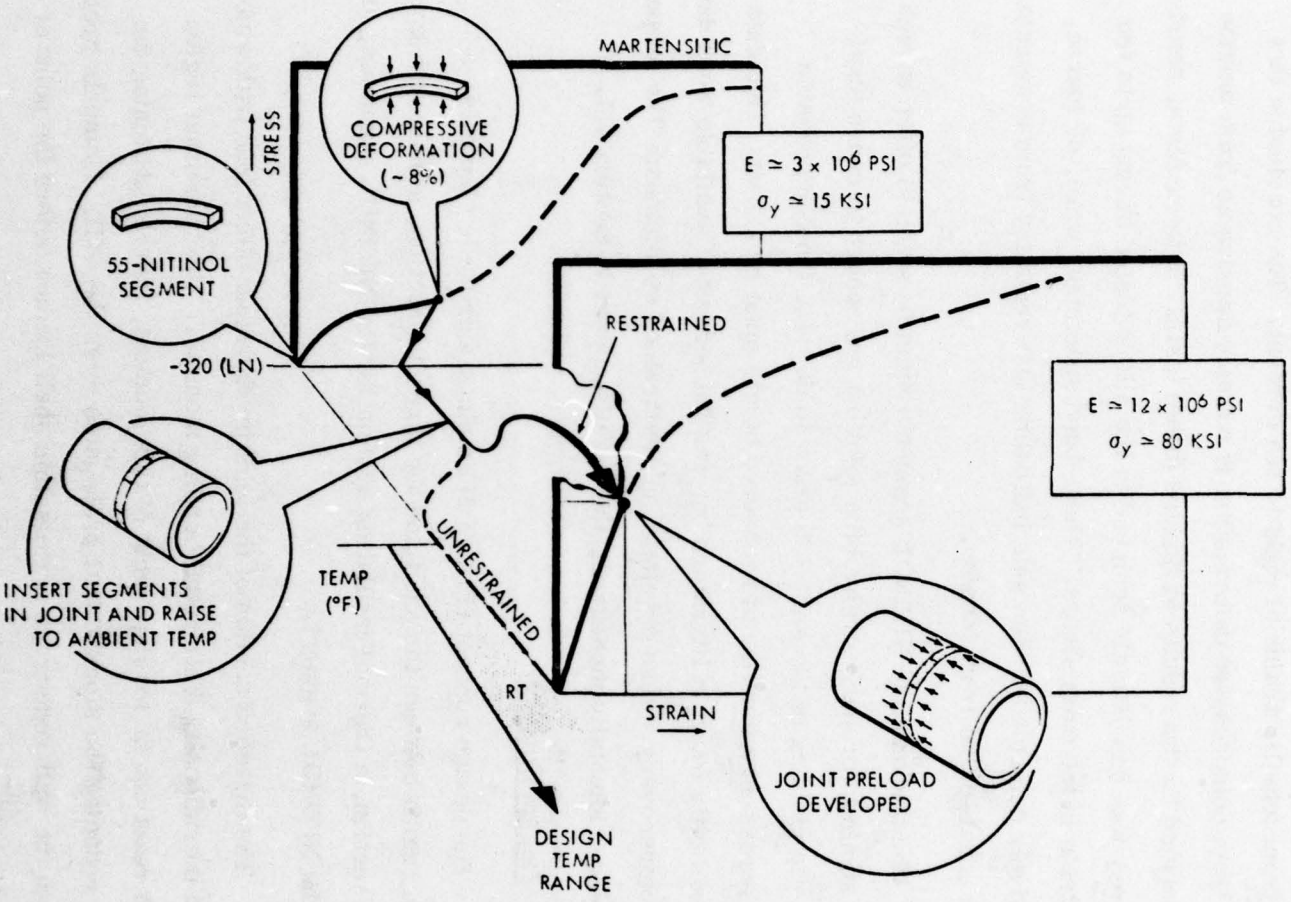

Figure 4. Stress-strain temperature history of NITINOL segment during preload development.

Limited test data (Reference 1) indicate that full recovery can be achieved from compressive strains of only four to six percent compared to full recovery from tensile strains of eight to ten percent. The conclusion that recovery from compressive deformation is not as extensive as from tension may be disputed by the results of flexure (bend) tests. In these tests, nearly full recovery was consistently achieved in the alloys tested having up to ten percent strain in the outer fibers. These bend specimens were, of course, compressively deformed on one side indicating that recovery from compressive strains is equal to that from tension.

The thickness of NITINOL segments must be sized to offer enough recovery strain to properly preload the joint but not enough to cause significant plastic yielding of the joint. In order to do this, the compressive recovery stress as a function of recovered strain must be known. This data was not explicitly found in literature but was backed out of available work data and data on recovery stress developed in constrained specimens. The property was also experimentally measured; the results appear in Section 5.1.

3.1.2 Design Concept

The design concept (Figure 5) employs four basic elements: a transition region between the shell and the threaded section, a male and female threaded section, a thermal insulation system for the NITINOL segments, and finally, the NITINOL segment.

The threaded section of the joint produces an offset load path which creates a meridionally distributed bending moment. The transition region serves to react out (in torsion) most of this moment, thereby stiffening the joint and reducing the moment that propagates down the wall. Moments propagated down the wall reduce the permissible shell loading before the point of incipient buckling.

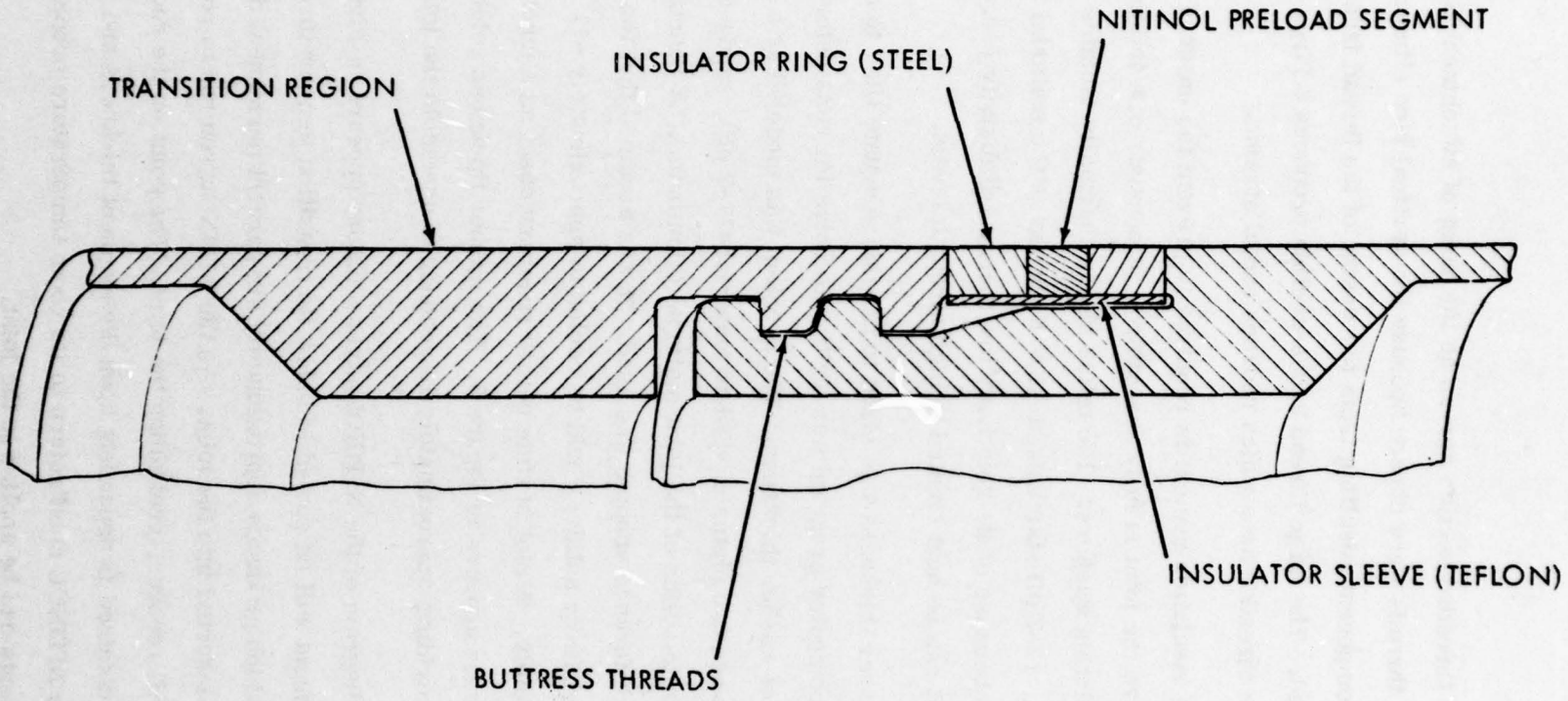

Figure 5. Design concept.

The threaded section serves as the point of attachment for the joint. Buttress-type threads were chosen because the vertical face eliminates the radial force component resulting from the cosine of the thread face angle and the applied load. The large thread cross-section produces a large section modulus in the threaded area which reduces radial strains.

The insulation system is required to prevent the onset of NITINOL recovery before the joint is fully assembled. It consists of a teflon sleeve and two steel insulating washers. The teflon sleeve thermally isolates the NITINOL from beneath. 17-7 pH stainless steel was chosen as the material for the steel washers because of its relatively low thermal diffusivity ($\sim 0.45 \times 10^{-5}$ M^2/sec) and it can be heat treated to high strength levels.

Washer thickness was sized to provide adequate time to assemble the joint. A computer program was written to solve for time before recovery as a function of washer thickness. The problem was modeled as a plate of NITINOL between two plates of washer material (17-7 pH), sandwiched between two semi-infinite solids of the joint material (aluminum). A Schmidt finite-temperature difference scheme was used. It was assumed that the joint halves (semi-infinite solids) would be cooled to approximately $-17^{o}C$ (0^{o} F) prior to assembly. A plot of time before recovery onset as a function of washer thickness appears in Figure 6. The washer thickness selected was 0.13-inch, providing approximately 14 seconds to assemble the joint.

A diagram of the NITINOL stress history appears in Figure 7. The NITINOL segment will be cooled to below its transition temperature, loaded to 100,000 psi which produces approximately six percent permanent deformation, unloaded and inserted into the joint. As the NITINOL returns to room temperature, it will recover, preloading the joint. The point on the recovery stress-strain curve obtained is dependent upon the segment thickness and joint compliance. The NITINOL must return to its room temperature properties before bending moments can be applied to the joint.

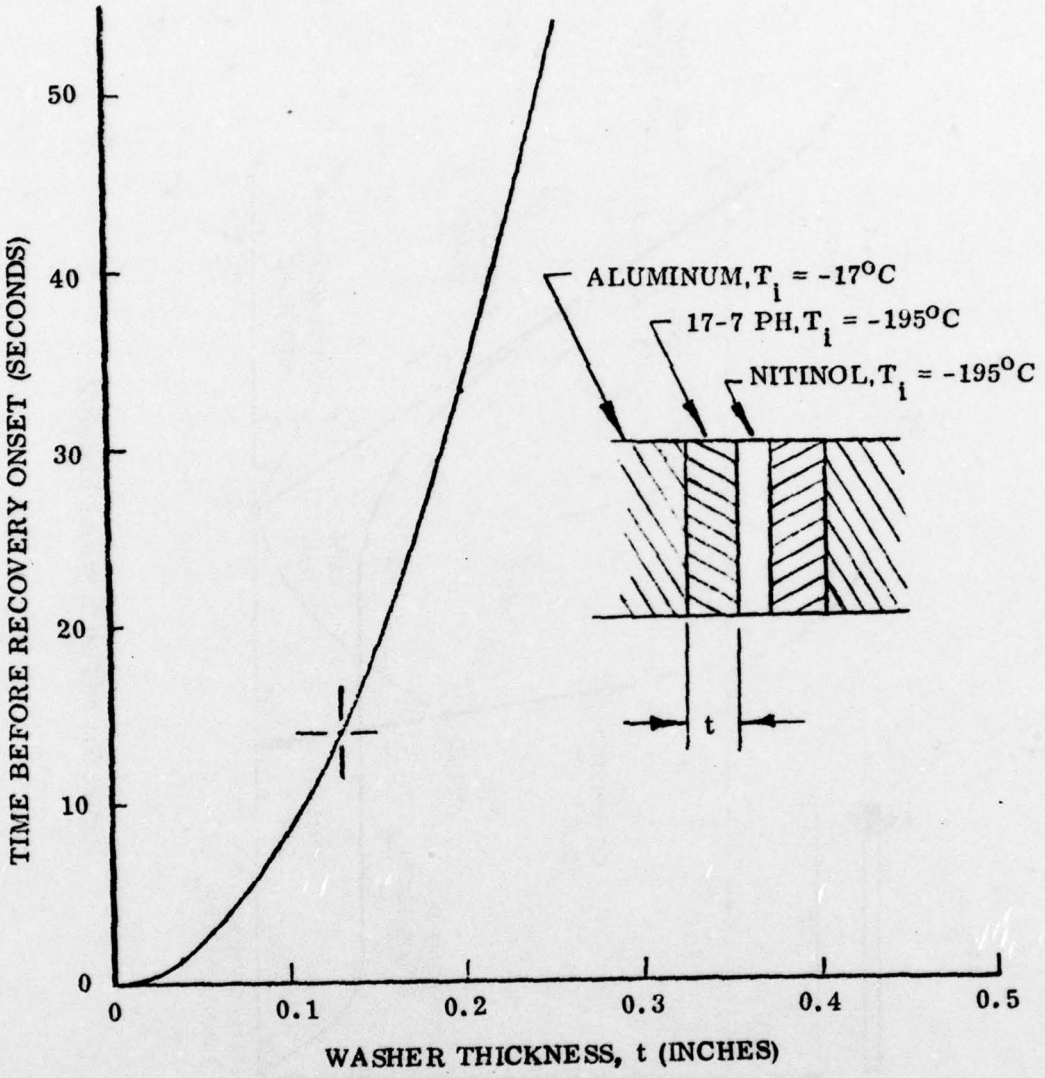

Figure 6. Time before recovery onset as a function of washer thickness, t.

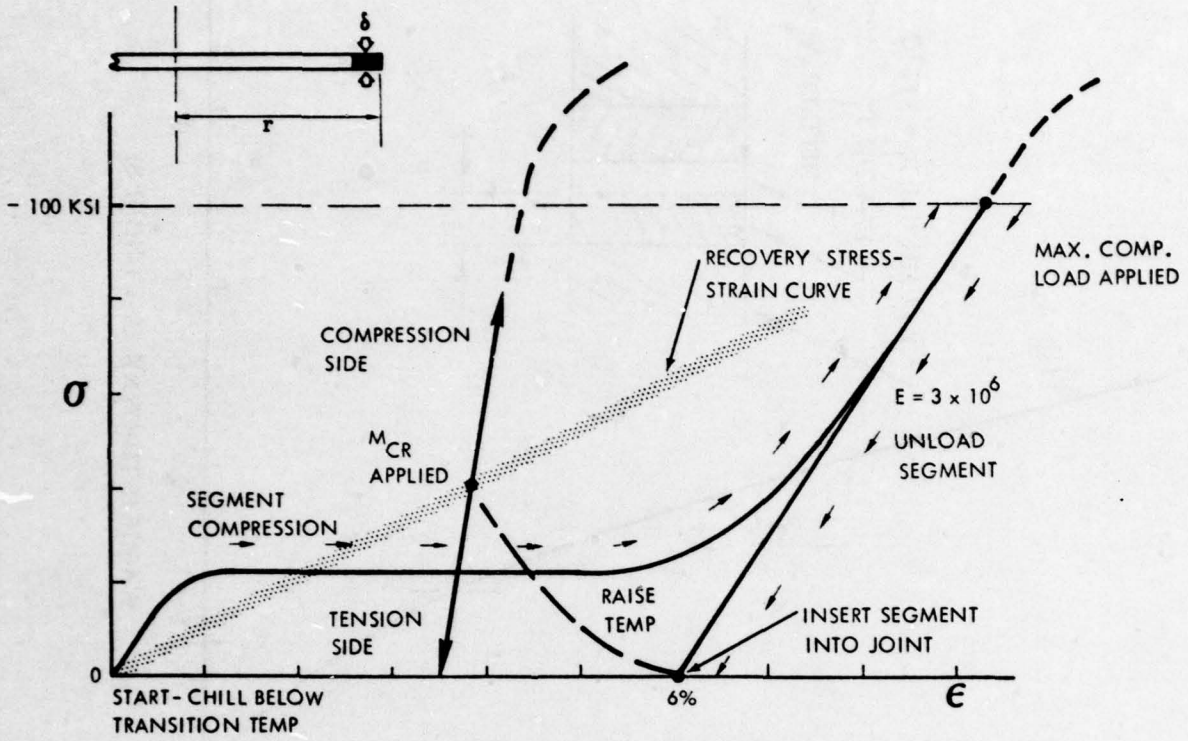

Figure 7. NITINOL stress history.

3.2 Comparison to Conventional Designs

Conventional methods of obtaining the required preload were examined; they included the conventional threaded joint preloaded with torque and a bolted flange joint.

3.2.1 Conventional Threaded Joint

Assembly torques required to produce the necessary preload in a threaded joint were estimated, accounting for a pressure-insensitive friction factor in the mating surfaces. The results show that very large torques are necessary. Two methods of applying these torques were analyzed; a very high friction strap wrench and a spanner wrench. For the eight inch diameter case, both methods resulted in structural failure of the joint and missile wall before the required preload torques could be obtained. A special spanner wrench might be developed and used to preload manufacturing joints, but it probably would not be practical to achieve this preload in the field.

3.2.2 Bolted Flange Joints

Bolted flange joints were sized using the optimum bolt size and spacing for each application. The following assumptions were made:

- The joint will fail from a stiffness standpoint if its preload is exceeded.
- Both the bolts and the flange are of a material with the same modulus (steel).
- NAS 624-644 bolts are used with NAS 1291 self-locking nuts.
- The bolts can be spaced no closer than a distance of 1.2 times the bolt heat diameter (Figure 8).
- The internal flange protrusion is equal to 1.2 times the bolt head diameter.
- The combined flange width (w) is equal to the internal flange protrusion.
- The bolts are torqued to 80 percent of their yield strength.

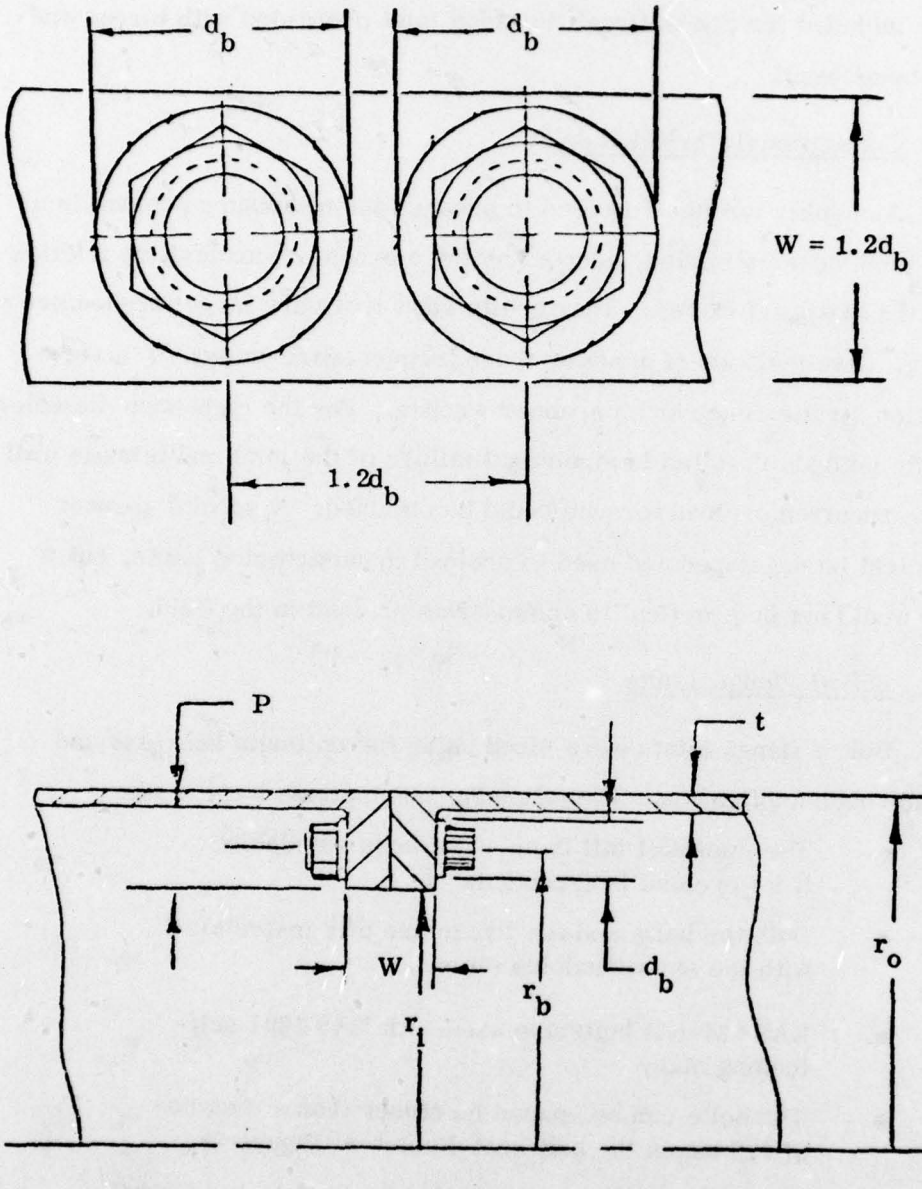

Figure 8. Bolted flange geometry.

- The joint is sized to maintain its preload under the stress induced by the critical bending moment which results in shell buckling of the missile case.

The numbers of bolts, minimum bolt size, and flange protrusion distances required to preload eight-inch diameter steel joints of various wall thicknesses, appear in Tables 1 and 2. It was shown that the joint could meet both strength and stiffness requirements; however, it is very unattractive from the standpoint of volume and protrusion and weight. It might also pose accessibility problems.

3.3 Alternate Design Concepts

Several alternate design concepts for NITINOL preloaded joints were conceived. They employed NITINOL in tension rather than compression. Three of the more promising concepts appear in Figure 9 along with their relative advantage and disadvantages.

One of three concepts, the sleeve-clamp, was selected for preliminary analysis using the finite element code NIFDI (Figure 10). The design uses a grooved band of NITINOL which will mate with grooves in the joint halves. Prior to installation, the band will be deformed approximately 5.5 percent, both longitudinally and circumferentially, in an LN_2 bath. It will then be slid over the body and positioned at the joint. As the NITINOL recovers, it will close both circumferentially and longitudinally upon the joint, preloading it. If this type of joint design is successful, it should be less expensive to manufacture than a threaded type joint and has the additional advantage that no relative rotation of one joint half to the other is required. Preliminary NIFDI results indicated that the concept was feasible, but additional iterative design and analysis will be required. Bi-axial recovery properties of NITINOL will have to be determined before detail design work can be performed.

TABLE 1. BOLT SIZES, MAXIMUM NUMBERS, AND MAXIMUM PRELOADS OBTAINABLE.

BOLT SIZE	N MAX. NUMBER OF BOLTS	F_b MAX. PRELOAD PER BOLT, lb.	F_bN MAX. TOTAL PRELOAD, lb.
2-56	60	481	28,860
4-40	48	780	37,440
6-32	40	1,183	47,320
8-32	34	1,820	61,880
10-32	29	2,600	75,400
1/4-28	22	4,732	104,000
5/16-24	18	7,540	135,700
3/8-24	15	11,414	171,200
7/16-20	13	15,431	200,600
1/2-20	11	20,787	228,700

TABLE 2. BOLT SIZE AND NUMBERS, PROTRUSION DISTANCE, AND FLANGE WEIGHT FOR VARIOUS WALL THICKNESSES.

WALL THICKNESS t, INCHES	BOLT SIZE	NUMBER N	PROTRUSION INCHES	FLANGE WEIGHT, lb.
0.02	2-56	15	0.20	0.28
0.04	2-56	60	0.20	0.31
0.06	10-32	26	0.40	1.23
0.08	5/16-24	17	0.62	2.96
0.10	1/2-20	11	0.98	7.03

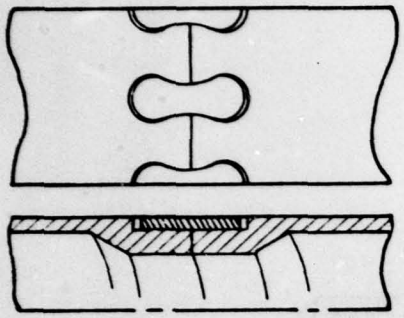

DOGBONE - TENSION

- MULTIPLE COMPONENTS
- TOLERANCES CRITICAL
- DIFFICULT MACHINING

SLEEVE CLAMP

- DETAILED ANALYSIS CONDUCTED
- MINIMIZE LOAD PATH OFFSET
- APPEARS PROMISING
- NITINOL ELEMENT IS DIFFICULT TO PRODUCE AND DEFORM PROPERLY

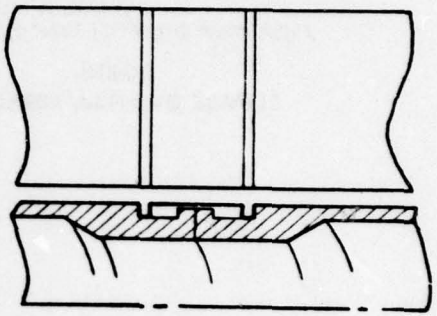

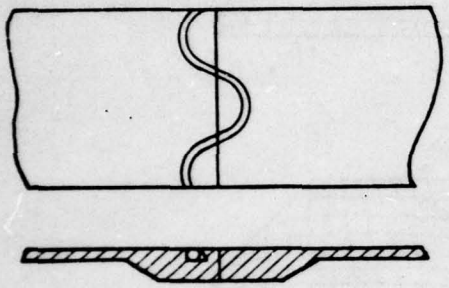

WIRE TENSION WRAP

- LOWER PRELOAD CAPABILITY
- SIMPLE INSTALLATION
- MINIMUM NITINOL USEAGE
- SIMPLE DISASSEMBLY

Figure 9. Alternate design concepts.

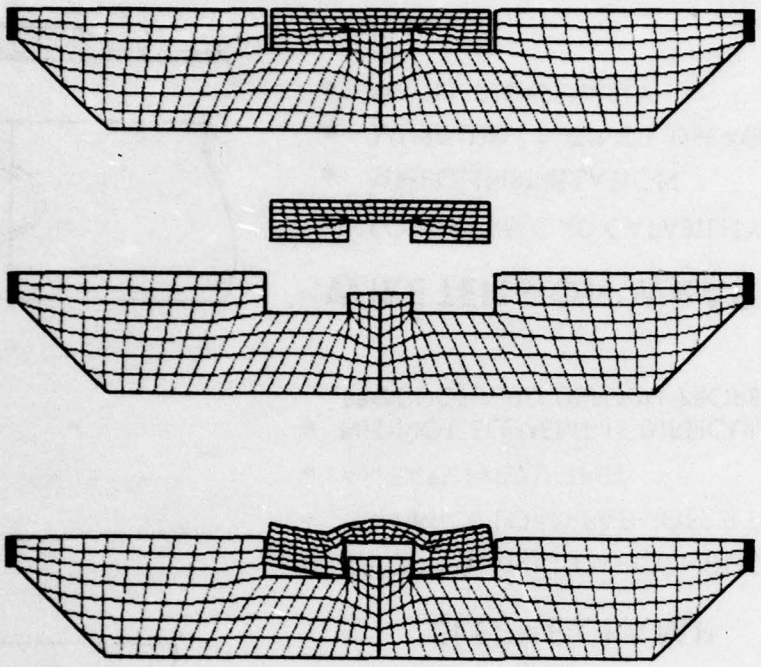

INTENDED ASSEMBLED CONFIGURATION

NITINOL BAND PRIOR TO ASSEMBLY

RECOVERY/PRELOAD RESULTS (NIFDI)

- ADDITIONAL ITERATIVE ANALYSIS/ DESIGN REQUIRED
- BI-AXIAL RECOVERY PROPERTIES REQUIRED FOR DETAILED DESIGN
- RESULTS INDICATE CONCEPT IS FEASIBLE

Figure 10. Sleeve-clamp analysis results.

4.0 ANALYSES

Analyses were performed in order to better understand the mechanisms of joint compliance, and in order to analytically iterate the baseline joint design. The finite element method was selected as the means of analysis, specifically the NIFDI finite element code. One-dimensional, closed form analytical techniques were completely inadequate since the actual stress states were at least two-dimensional. An analytical behavior model for NITINOL recovery was developed. Performance of both the baseline NITINOL and torque (conventional) preloaded joints was predicted. An eight-inch diameter joint was also analyzed in order to determine the effect of scaling on joint compliance.

4.1 NIFDI Finite Code

The advantages of the finite element method over other methods are numerous. The finite element method affords nearly complete generality in the specification of geometrical and material properties; i.e., geometrically complex bodies of many different materials are easily represented. Displacement or stress boundary conditions can be specified at any node of the finite element system. Thermal and mechanical loads, as well as initial displacements, can be specified at nodes and, if the number of nodes is sufficient, nearly arbitrary distributions of the loads and displacements can be represented. In addition, the body as a whole can be subjected to accelerations and/or angular velocities.

The NIFDI finite element can be applied to the determination of displacements, stresses, and strains in arbitrary axisymmetric and plane bodies which may have jointed frictional interfaces. Orthotropic temperature-dependent material models for either bilinear plasticity or unequal properties in tension and compression are included. The bodies can be subjected to arbitrary axisymmetric mechanical, thermal, and pore pressures, as well as initial

displacements. The mechanical loads can be surface pressures, surface shears, and nodal point forces, as well as acceleration or angular velocity.

The version of Stress Analysis of Axisymmetric Solids (SAAS) used is titled NIFDI (Nonlinear Analysis of Interfaces with Friction between Discontinuous Solids having Interference Fit). NIFDI is based on extensive use of SAAS III and contains revisions which increase its capability.

The SAAS III program's capability was improved by the introduction of equivalent loads due to initial displacements and interface elements to account for jointed frictional interfaces. The bilinear plasticity solution capability was updated to include additional iterative solution logic necessary when interface elements are specified. Features include temperature interpolation restart and multiple case capability, skew boundaries, elastic-plastic analysis, plane stress/plane strain options, unequal properties in tension and compression, and porous media option.

NIFDI is uniquely suited for analysis of threaded interfaces. Plasticity, thread contact surface load transfer with friction and initial loads due to makeup torques or NITINOL shape recovery can be included in the analysis. A one-dimensional interface element is used to model the transfer of load between threaded interfaces. The code contains an iterative solution technique to account for nonlinear effects arising from plastic stress-strain behavior, friction and geometric discontinuities. Deformed element plots (with deformation magnification) can be output to illustrate behavior under load. The code proved a very useful tool in determining sources of compliance and stresses caused by the offset load path, as well as overall joint and thread form optimization. A shortcoming of the NIFDI is that moments could not be applied directly; so the maximum stresses (tensile and compressive) resulting from the application of a given moment were calculated and converted into tension and compression loads which were applied to the model. Strains resulting from these loads were then used to calculate joint stiffness.

4.2 NITINOL Behavior Modeling

The thickness of NITINOL segments must be sized to offer enough recovery strain to properly preload the joint but not enough to cause significant plastic yielding of the joint. In order to do this, the recovery stress as a function of recovered strain must be known. This data was not explicitly found in literature but was backed out of available work data and data on recovery stress developed in constrained specimens (Reference 1). Figure 11 illustrates the recovery stress-strain curve backed out of literature and the simplified curve used for analysis. The accuracy of these curves was verified experimentally for compressive recovery properties (Section 5.1, NITINOL Characterization Tests). The recovering NITINOL behaved almost like an ordinary material having a modulus of 1×10^6 psi; that is how it was modeled.

The memory characteristics of NITINOL were treated in the NIFDI code as follows: the recovery stress as a function of recovered strain was input into NIFDI by assigning the NITINOL elements an initial displacement equal to the amount that the actual segment was to be deformed prior to installation (eight percent) and modulus of elasticity, $E = 1 \times 10^6$ psi. A case was run with these properties to determine the initial preload conditions of the joint. Once the initial preload conditions were known, they were converted to a series of initial displacements that were input along with the room temperature properties of NITINOL ($E = 12 \times 10^6$ psi, $\sigma_{yp} = 80,000$ psi). The joint was then loaded in tension and compression and its stiffness, stresses and residual preload as a function of applied load were determined.

4.3 Baseline Joint Iteration

A 4.0-inch diameter by 0.060-inch wall aluminum joint was selected as the baseline case. This configuration is similar to a tactical missile structure.

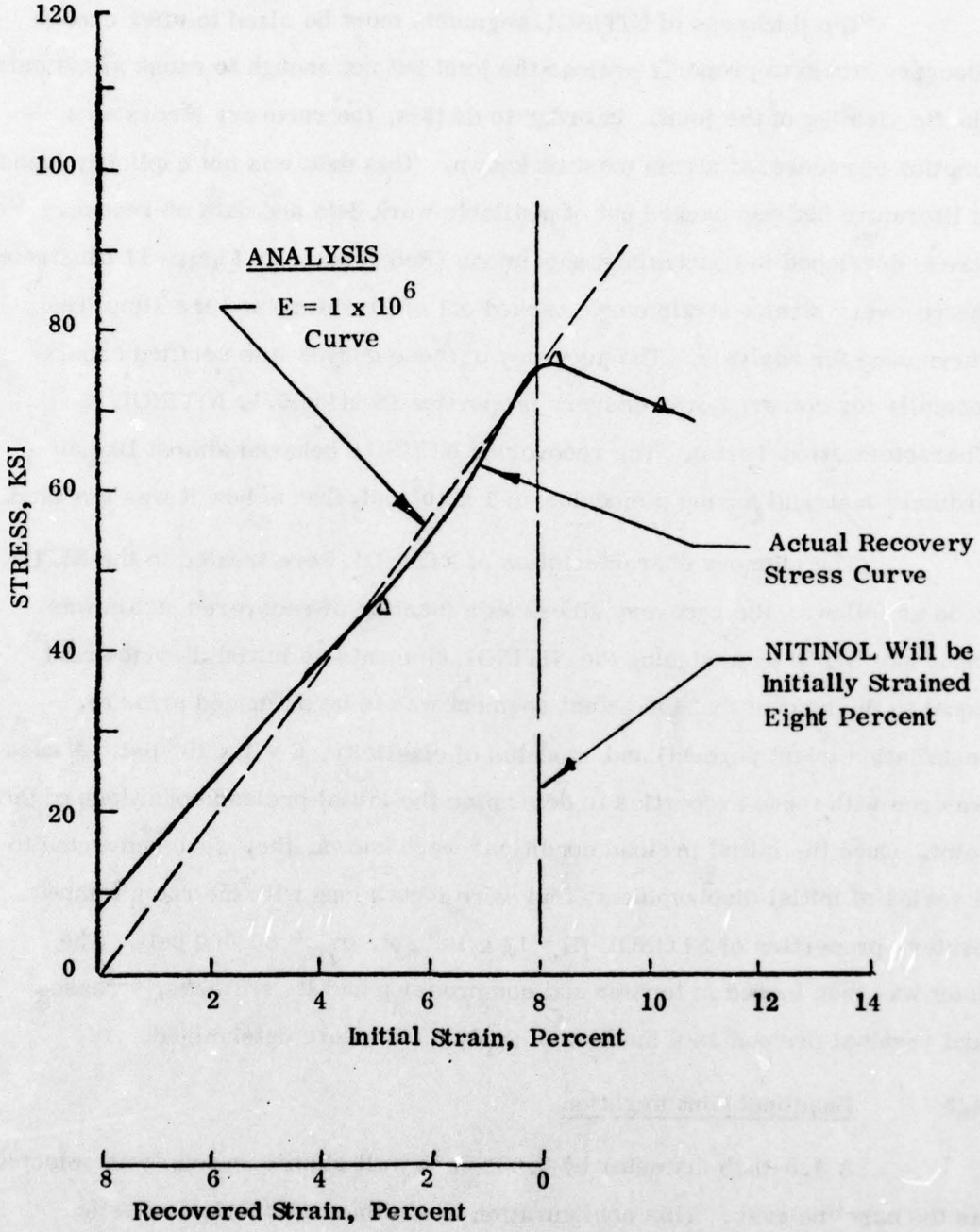

Figure 11. Recovery stress-strain curve for NITINOL (dervied from Reference 1).

The basic design criteria was that the joint be at least as stiff as the surrounding shell, to a load equal to the critical moment (M_{cr}) resulting in incipient shell buckling. For the baseline aluminum joint, that moment was 29,000 in-lb. In order to maintain the required stiffness to that load, a pre-load exceedance moment (M_{pe}) of 24,000 in-lb was selected as the design goal.

The original threaded joint (Figure 12) was designed using the one-dimensional closed form equations. The NIFDI plot of the same joint loaded in tension shows large deflections; mostly the result of strains in the meridional direction, thus demonstrating the three-dimensional nature of joint compliance which cannot be adequately described with one-dimensional equations. Large bending moments propagated down the missile wall on both sides of the joint. This is an undesirable situation since the moments will reduce the permissible shell loading before the point of incipient buckling (M_{cr}). It was found that the largest stresses occurred across Section AA and were due to combined bending and tension.

Several design changes were made before the final baseline joint configuration was selected. Figure 13 illustrates the element plot and deformed structure plot of the final baseline joint in the unloaded and loaded to 24,000 in/lb, respectively. Also shown are calculated stresses at critical areas for the loaded and unloaded conditions. An area of thickened cross-section is on both the male and female sides of the joint. It serves to carry (in torsion) most of the moment caused by the offset load path, thereby stiffening the joint and reducing the moment that propagates down the missile wall. The thread form chosen is one defined by the American Petroleum Institute (API) (Figure 14). It is used for buttress threads on oil casing. It was selected for two reasons: one, it has a very shallow pressure angle on the contacting faces so the radial component of thread contact pressure is minimal; two, its form is one of proven abuse resistance and thus suitable for field operations. It was found that most of the load is carried through the first thread interface.

a. Not Loaded

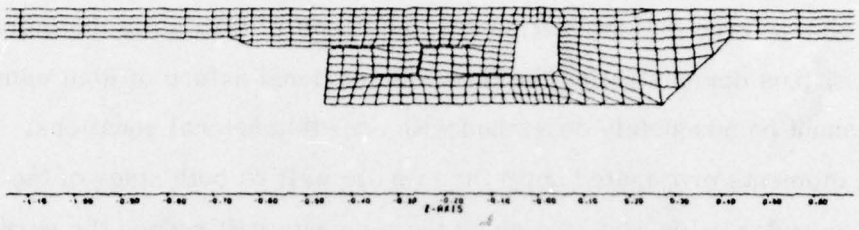

b. Loaded in Tension

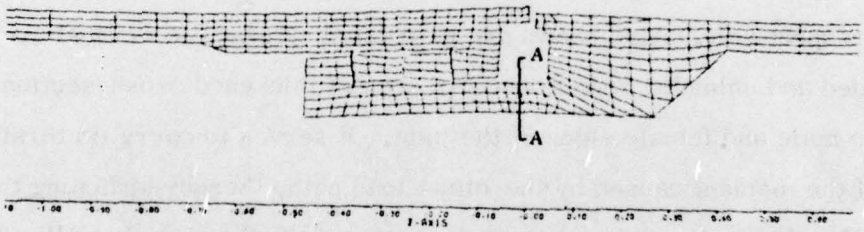

Figure 12. Original threaded joint.

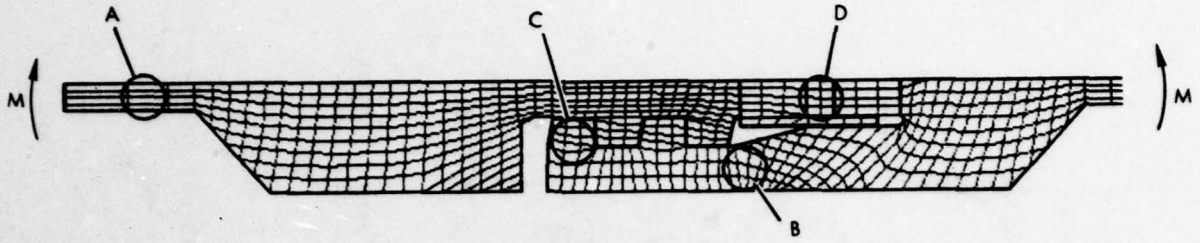

TENSION SIDE

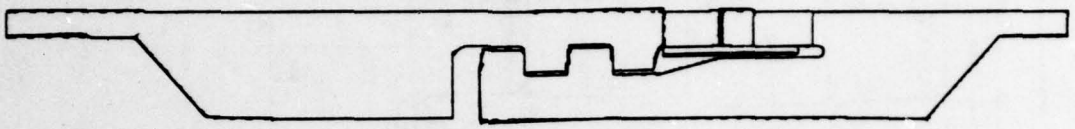

- TRANSITION REGION SIZED FOR REDUCTION AT OFFSET MOMENT IN SHELL

STRESS SUMMARY
(ALUM. 4" DIA. TEST ARTICLE)

LOCATION	M = 0	M = M_{CR}	
		TENSION SIDE (PSI)	COMPRESSION SIDE (PSI)
A (AXIAL)			
- I.D.	0	+22,000	-58,570
- O.D.	0	+16,000	-18,700
B (AXIAL)			
- I.D.	- 9,345	-11,150	- 7,555
- O.D.	+57,500	+63,000	+11,237
C (SHEAR)	+ 3,280	+ 9,650	0
D (AXIAL)	-22,000	0	-46,800

Figure 13. NIFDI analysis results.

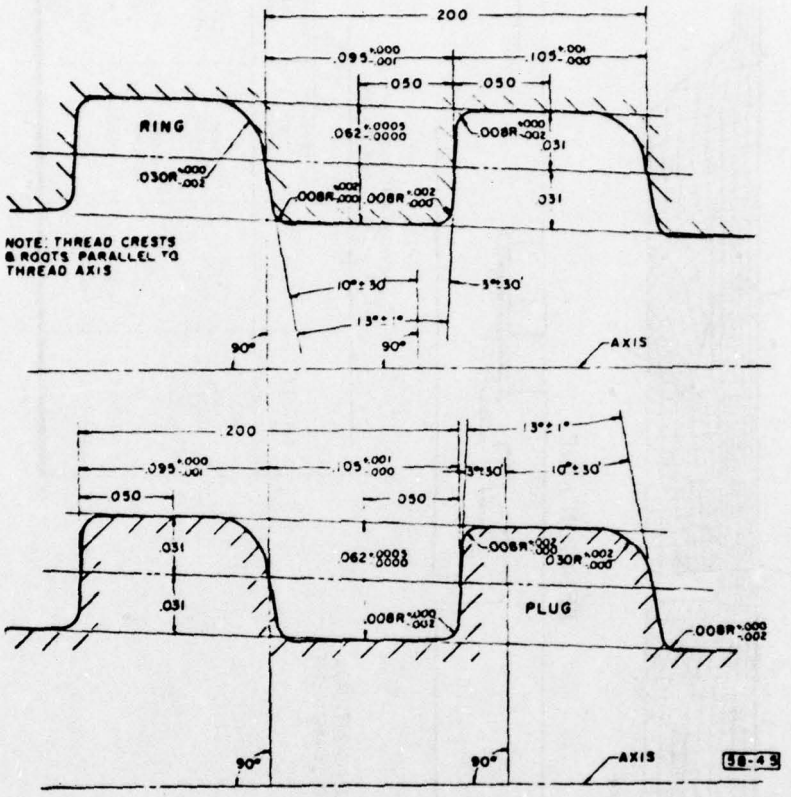

Figure 14. API thread form.

The load is not efficiently distributed when many threads are used and the length of the threaded section provides compliance. Therefore, a joint having only 2-3 threads was selected. The model analyzed had only two threads since that is the minimum number in contact.

The NITINOL segments preload the joint to approximately 75 percent of the critical load (P_{cr}) which is taken to be the maximum meridional load resulting from the application of a bending moment equal to M_{pe}. When loaded in tension to P_{cr}, the load has just lost its preload. At that load, some localized yielding occurs during the first loading cycle; however, the joint still performs as required. The overall joint stiffness is approximately 75 percent higher than the surrounding shell.

Joint stiffness as a function of applied moment appeared in Figure 15 for the baseline NITINOL preloaded joint, the surrounding no-joint shell structure, and the baseline joint preloaded with 200 ft/lbs of torque only. Stiffness (M/θ) is defined as the applied moment (M), divided by angular change per inch of length of the structure (θ/in). Units of in-lb/rad/in or in^2-lb/rad are used, which is analogous to the units of modulus of elasticity. times moment of inertia (EI). For the no-joint structure, stiffness is constant to the point of wall buckling or yield point, whichever comes first.

The joint has one modulus when it is preloaded and a lower one when the preload has been exceeded. As the bending moment is increased, the preload is not exceeded completely across the entire joint, but starts at the point furthest from the neutral axis and works its way down. The stiffness asymptotically approaches that of the completely un-preloaded joint.

4.4 Conventional Threaded Joint

The baseline joint configuration preloaded with torque only was analyzed. The amount of preload (P) obtainable via torque was calculated by the equation:

$$p = \frac{T}{\pi \mu D^2}$$

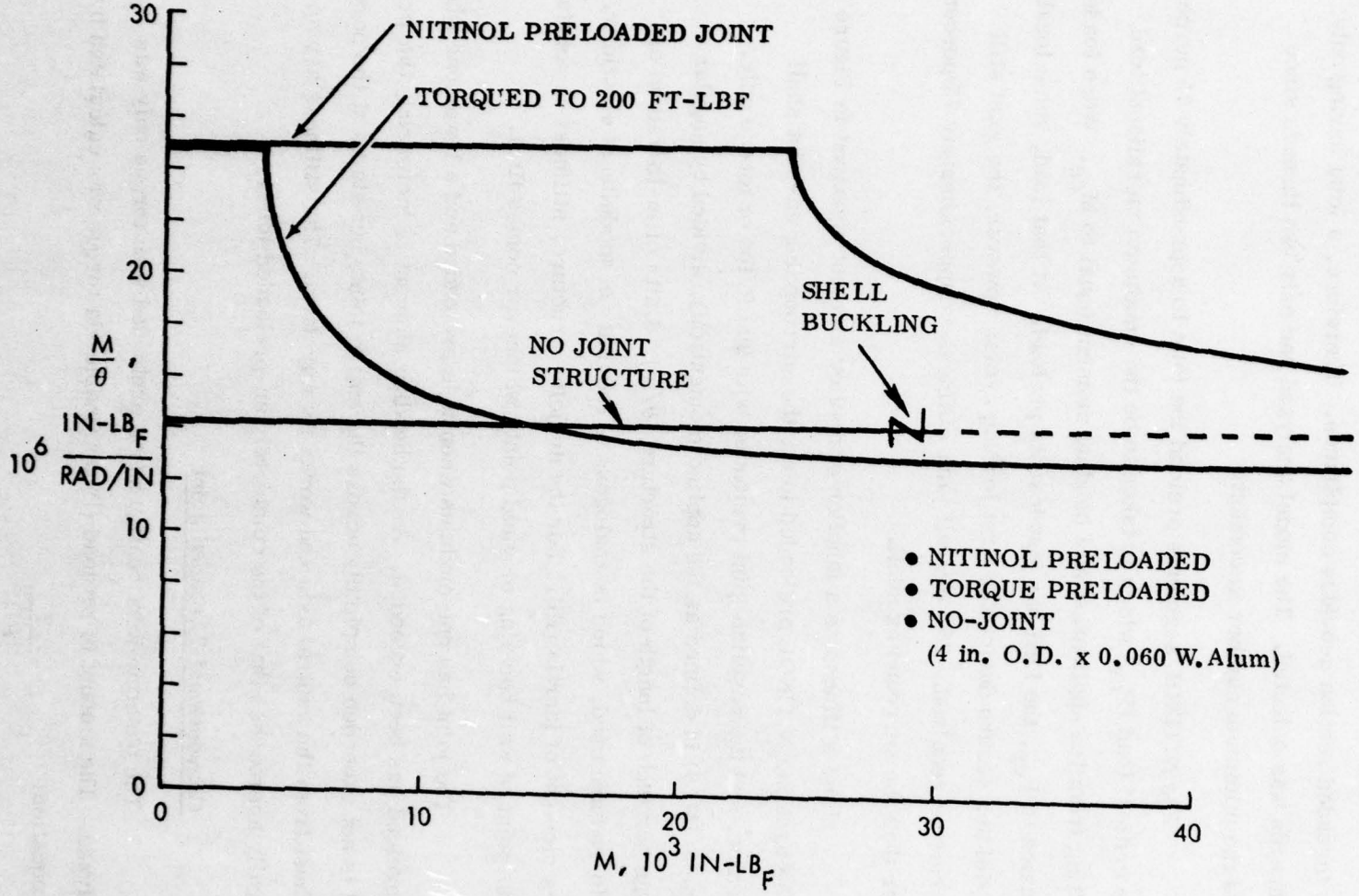

Figure 15. Joint stiffness as a function of applied moment.

where μ = friction coefficient

T = torque (in-pounds)

D = diameter of the joint (inches)

p = preload in meridional pounds per inch.

A friction coefficient for lubricated surfaces was assumed (0.15). The joint was preloaded with 200 ft-lbs of torque. Its stiffness characteristics also appear in Figure 15. M_{pe} was only 15 percent of that for the NITINOL joint.

4.5 Scaling Effects

NIFDI cases were also run on an eight inch diameter joint having the same wall thickness and joint dimensions as the baseline case, but made of steel. This configuration is similar to a torpedo body (Figure 16).

The torque required to achieve a given preload goes up as the square of joint diameter. Thus, four times as much torque would be required for an eight inch diameter joint as compared to the four inch joint.

Joint compliance also increases with the square of the diameter; so maintaining a preload is very important. NITINOL preloading appears to provide even greater stiffness improvement over conventional threaded joints as the diameter-to-wall thickness ratio is increased.

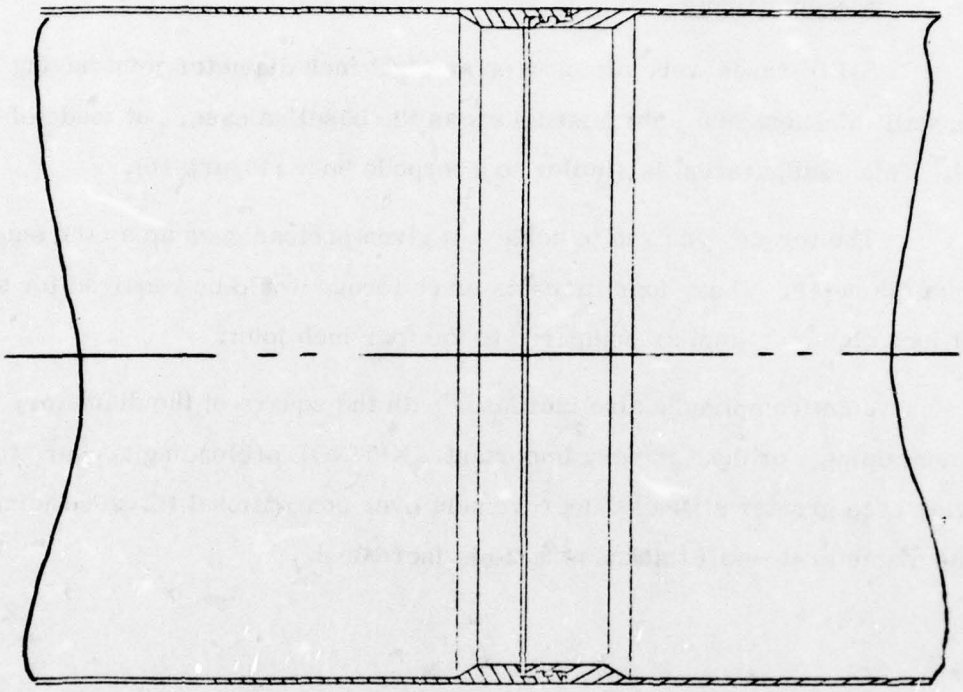

Figure 16. Eight-inch NITINOL preloaded joint (1/2 size).

5.0 TESTING

During performance of the contract, a series of tests were conducted; these included tests of NITINOL characteristics, conventional (torque preloaded) joint performance, and NITINOL preloaded joint performance.

The NITINOL characterization tests served to verify the compressive recovery model used for joint design and analysis.

Conventional joint tests were done using a model of the baseline joint preloaded with torque only. They served as a comparison to analysis and the NITINOL preloaded joint. Quantities measured included preload, preloaded stiffness, the moment causing preload exceedance (M_{pe}), and strains at various locations.

The NITINOL preloaded joint was successfully assembled and tested. The joint exhibited large improvements in preload and stiffness and a 17-fold increase in M_{pe} over the conventional joint. The preload level achieved agreed closely to that predicted by NIFDI.

The tests successfully demonstrated the feasibility of NITINOL preloaded joints. It was shown that very large performance improvements in joint stiffness could be achieved through NITINOL preloading.

5.1 NITINOL Characterization Tests

5.1.1 Purpose

The purpose of NITINOL characterization tests was to verify the recovery model used for the analyses; that required determination of recovery stress as a function of unrecovered strain. This data was not explicitly found in literature but was backed out of available work data and data on recovery stress developed in constrained specimens. Because of the uncertainty in this and because most of the available data deals with specimens

yielded in tension rather than compression, it was necessary to measure this property using samples of NITINOL from the S-3 billet.

5.1.2 Apparatus

Apparatus consisted of NITINOL samples, a compression fixture and a device for measuring recovery stress and strain.

The NITINOL samples were machined from strips which were received prior to receipt of the two NITINOL plates from which the actual joint ring was made. They were said to have been edge cuts from the S-3 billet material after processing. The samples had a planform area of 0.05 $inch^2$ and were 0.070 inch thick.

The compression fixture consists of two precision ground 1/2-inch thick steel plates, drawn together with 1/2-inch - 20 bolts. Stop blocks were used to limit the amount of NITINOL deformation. The blocks are made of hardened tool steel and ground to the proper dimension. This dimension is the NITINOL sample thickness less the eight percent desired deformation; less the elastic deformation of NITINOL at its yield point in LN_2:

$$\frac{\sim 25,000 \text{ psi}}{3 \times 10^6} = 0.8 \text{ percent}$$

The fixture is surrounded by an insulated container which can be filled with LN_2 for cooling. The device used for measuring recovery stress and strain appears in Figure 17. It consists of a set of dial indicators to measure total strain and a hydraulic cylinder used to apply a load. That cylinder was backed against a load beam. The compliance of the load beam served to maintain a relatively constant stress level in the NITINOL independent of small changes in sample displacement.

5.1.3 Procedure

The test procedure was as follows:

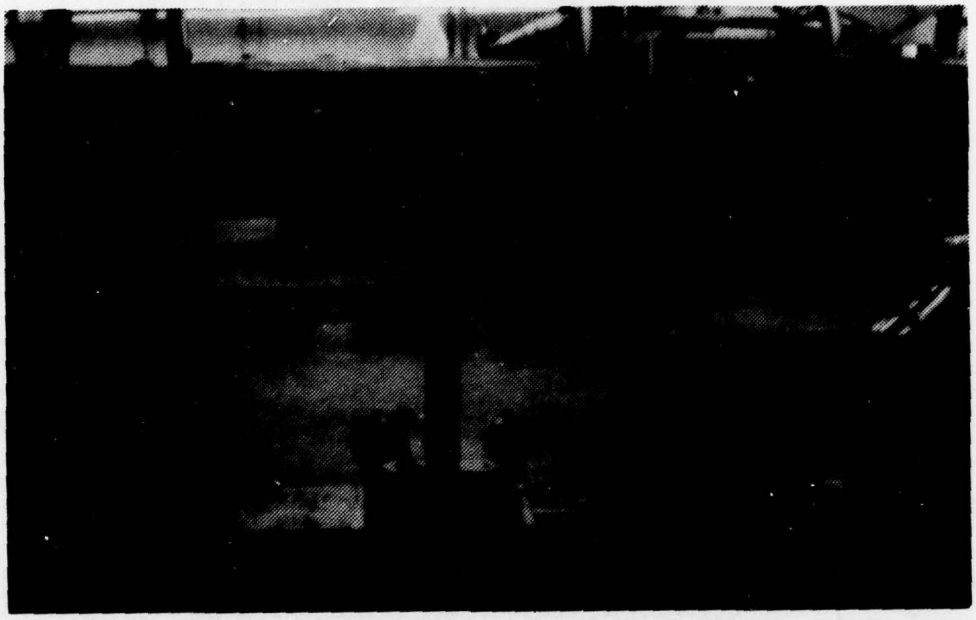

7900120

Figure 17. Test apparatus used for tests of recovery stress as a function of recovered strain.

1. The NITINOL sample's dimensions were measured and recorded, along with the dimensions of the stop blocks.

2. The NITINOL sample and stop blocks were placed in the compression fixture.

3. The fixture was placed in an LN_2 bath and soaked for 10 to 15 minutes.

4. The bolts were tightened to over 30 ft-lbf of torque and then removed.

5. The entire fixture was removed from the LN_2 bath and placed under the load beam where the dial indicator holder was placed over it. The assembly was then hydraulically loaded to the desired stress level.

6. The dial indicators were zeroed.

7. Indicators were read several hours after the sample had come to room temperature.

8. In cases where the stress level was above 40,000 psi, the samples were heated to approximately 200°F and allowed to cool for several hours before readings were taken.

9. Loads were recorded (stress level).

5.1.4 Results

Recovery stress was calculated directly from the applied load. Recovered strain was obtained by averaging the indicator readings, subtracting out thermal expansion of the compression fixture between LN_2 temperature and room temperature, and then dividing the NITINOL sample thickness. The recovered strain was then subtracted from the initial strain to obtain the amount of strain that was not recovered (unrecovered strain).

In all, five data points were obtained; a plot of these, along with one documented point,appears in Figure 18. The measured data agrees closely to that which was backed out of published work data.

Recovery temperature is a function of the stress level and for stress levels above 40,000 psi, the recovery temperature was above room

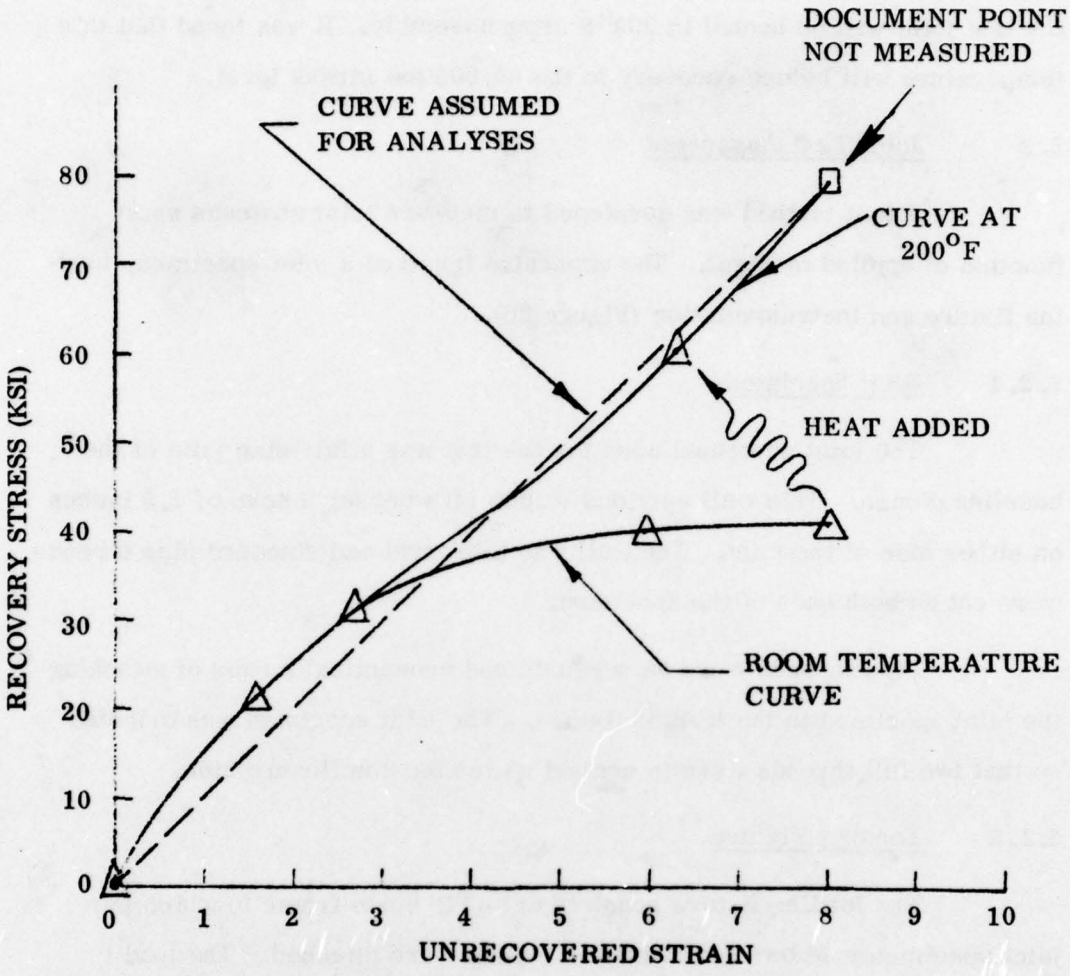

Figure 18. Recovery stress as a function of unrecovered strain for the NITINOL, S-3 billet material (original strain ≅ 8 percent).

temperature. This effect has been documented (Reference 1). A graph of its effect on 55-NITINOL wire appears in Figure 19. To insure full recovery, the test joint will be heated to 200°F after assembly. It was found that this temperature will induce recovery to the 60,000 psi stress level.

5.2 Joint Test Apparatus

A test method was developed to measure joint stiffness as a function of applied moment. The apparatus involved a joint specimen, loading fixture and instrumentation (Figure 20).

5.2.1 Joint Specimen

The joint specimen used for the test was a full-size joint of the baseline design. Thin wall sections (0.060 in) went for a span of 2.5 inches on either side of the joint. The wall was thickened and standard pipe threads were cut on both ends of the specimen.

Pipe threads were an adequate and economical means of attaching the joint specimen to the loading fixture. The joint specimen was oriented so that two full threads were in contact on the tension flexure side.

5.2.2 Loading Fixture

The loading fixture consists of an "I" beam frame to which the joint specimen load bar and hydraulic cylinder are attached. The load is applied along the load beam by a hydraulic cylinder of known area and a hand-operated hydraulic pump. A calibrated pressure gage is used to measure the load (Figure 21). The load can be placed at various locations along the load bar in order to vary the moment shear relationship at the joint.

5.2.3 Instrumentation

In order to measure joint stiffness as a function of applied moment, both the applied moment and joint deflections must be known. The moment was calculated from the calibrated pressure gage reading and the measured

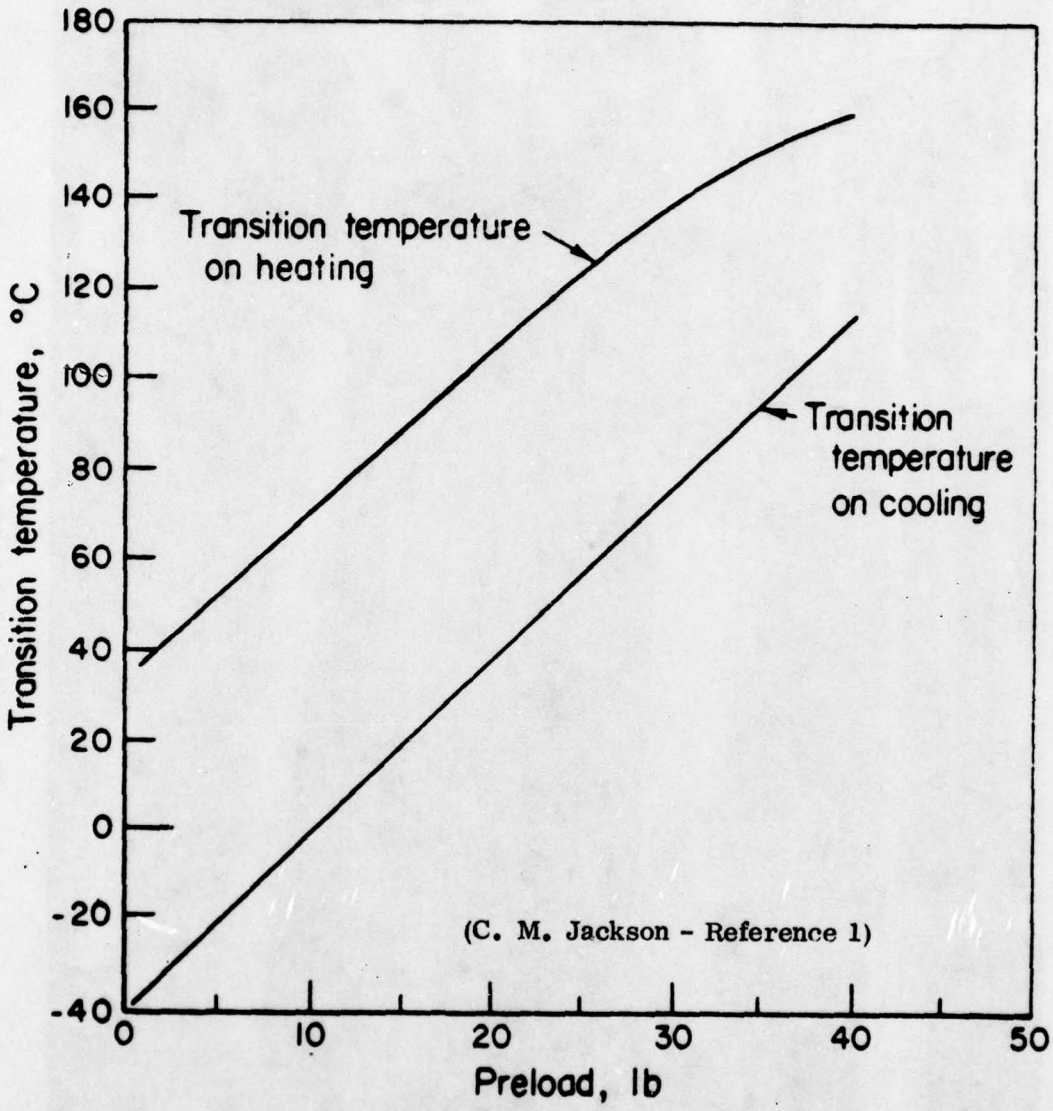

Figure 19. Effect of preload weight on transition temperature. (observed for 0.026-in.-diameter 55-NITINOL wire containing 44.6 weight percent Ti and 0.07 weight percent C)

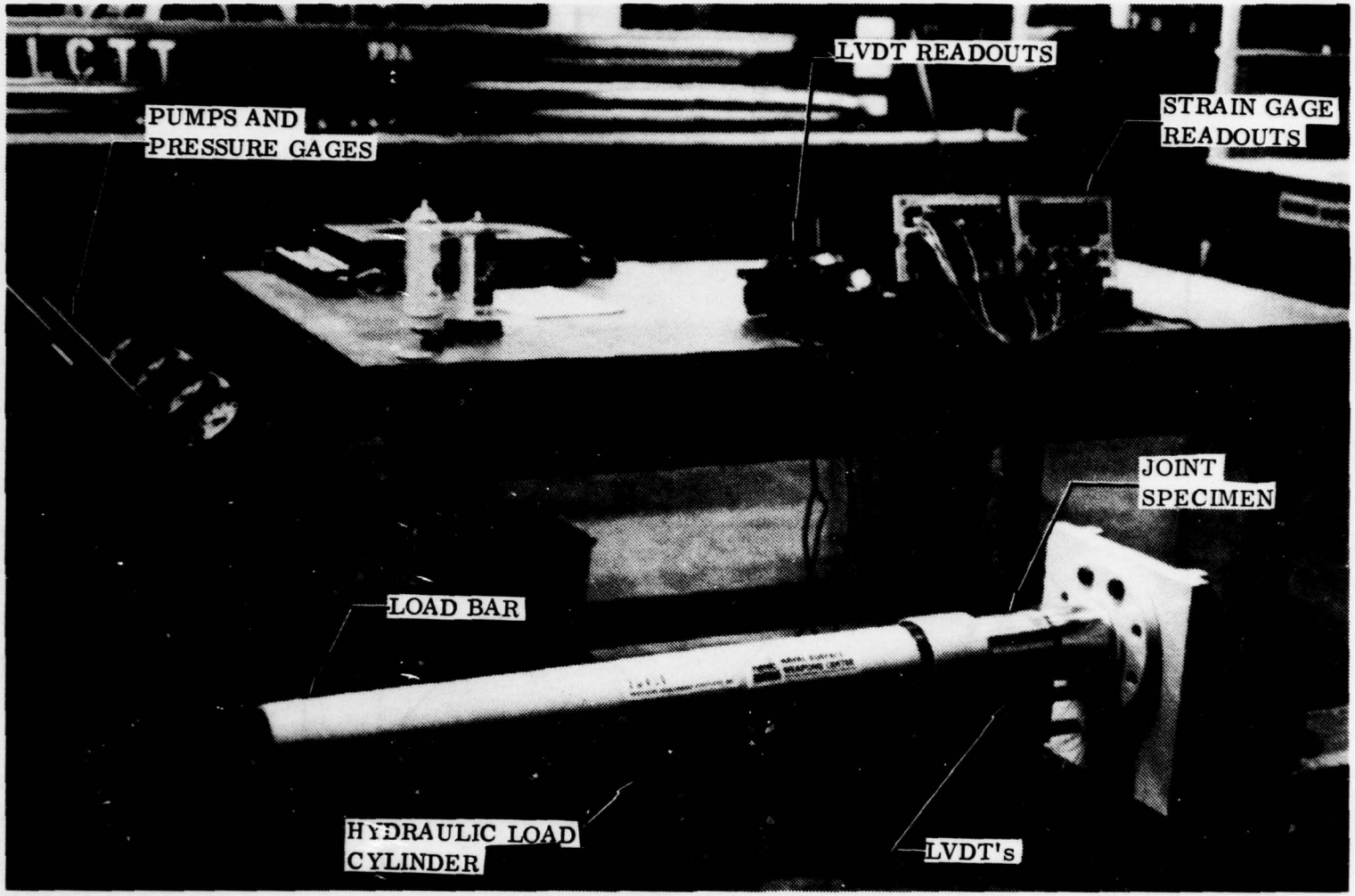

Figure 20. Joint test set-up.

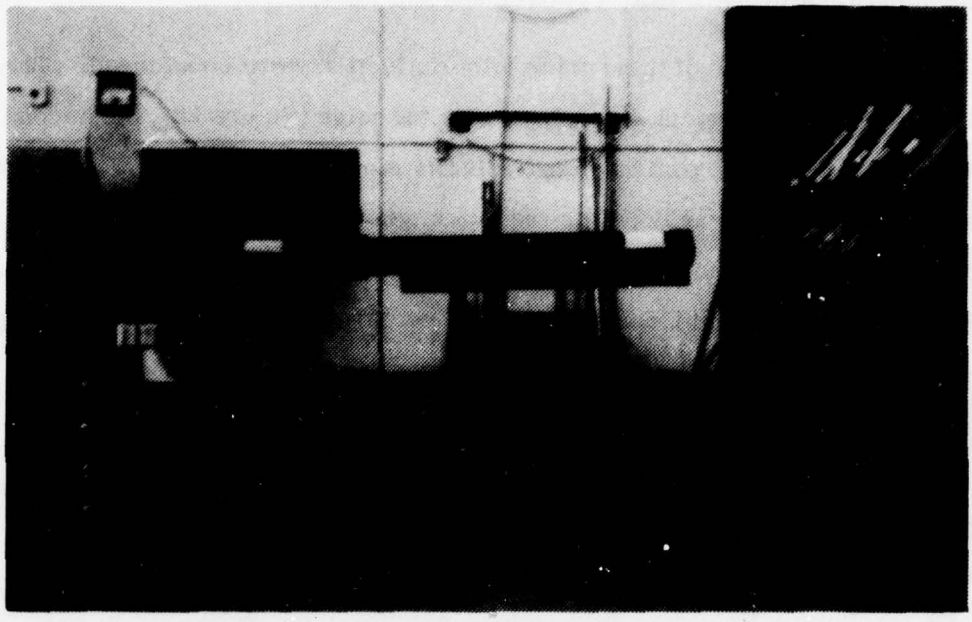

LOAD BEAM AND SUPPORTING STRUCTURE

CALIBRATED HYDRAULIC PRESSURE GAUGES 7900119

Figure 21. Test joint loading fixture.

distance between the hydraulic cylinder and the joint.

Two methods of measuring joint deflection were considered. The first involved measurement directly across the joint (Figure 22); the second required two indicator readings longitudinally along the specimen (Figure 23). An accuracy analysis was done for the two methods taking into account the readability and linear accuracy of the LVDT's. It was found that the full load deflection of the joint could be determined to within ± one percent using the first method. The second method was rejected because although joint deflections are magnified by spacing the displacement pick up further from the joint, the shell deflections must be accurately known and subtracted out of the readings. The NIFDI analysis indicated that these deflections would be significant, thus adversely affecting the accuracy of the method.

The LVDT's selected were Schaevitz type 100 DC-D. Coupled with an electronic digital volt meter, the system readability was ± one millionth of an inch. Linearity is 0.25 percent of full range. The derivation of joint rotation as a function of LVDT reading is as follows (reference Figure 22):

r	=	radius of joint to outer surface
d_1	=	radial distance from joint surface to LVDT-1
d_2	=	radial distance from joint surface to LVDT-2
d_3	=	distance between LVDT attachments
δ_j	=	axial deflection at joint surface
δ_1	=	axial deflection of LVDT-1
δ_2	=	axial deflection of LVDT-2
θ	=	angular rotation of joint (radians / inch)
θ_L	=	rotation of joint surface at LVDT attachment (left side)
θ_R	=	Ibid (right side)

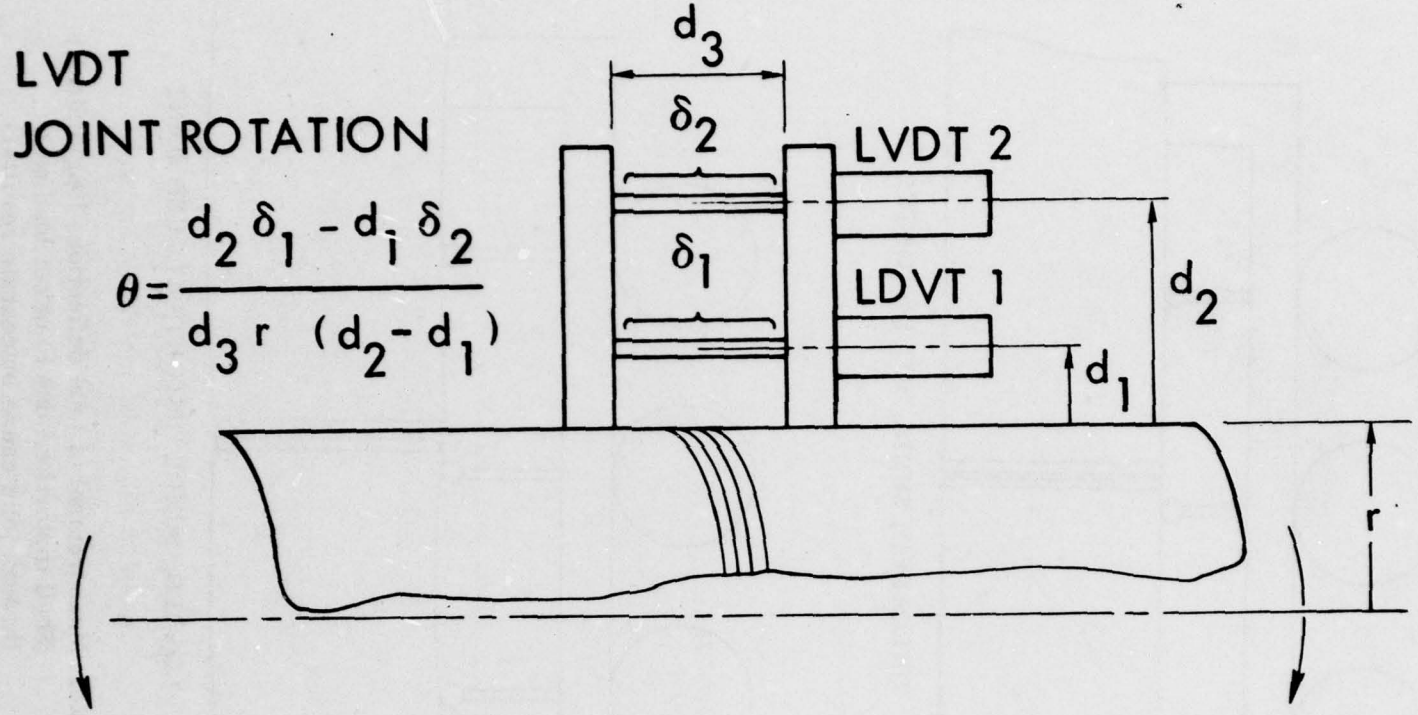

Figure 22. Method of measuring joint rotation for stiffness calculations.

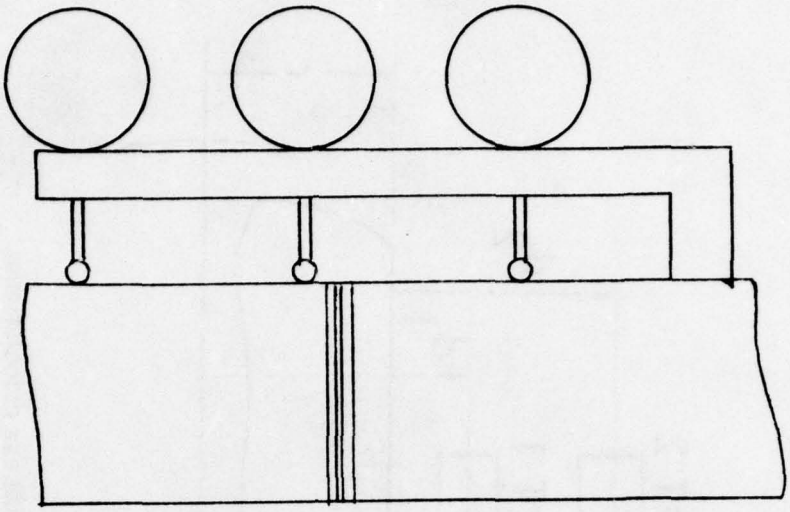

UNLOADED, SHELL NOT DISTORTED

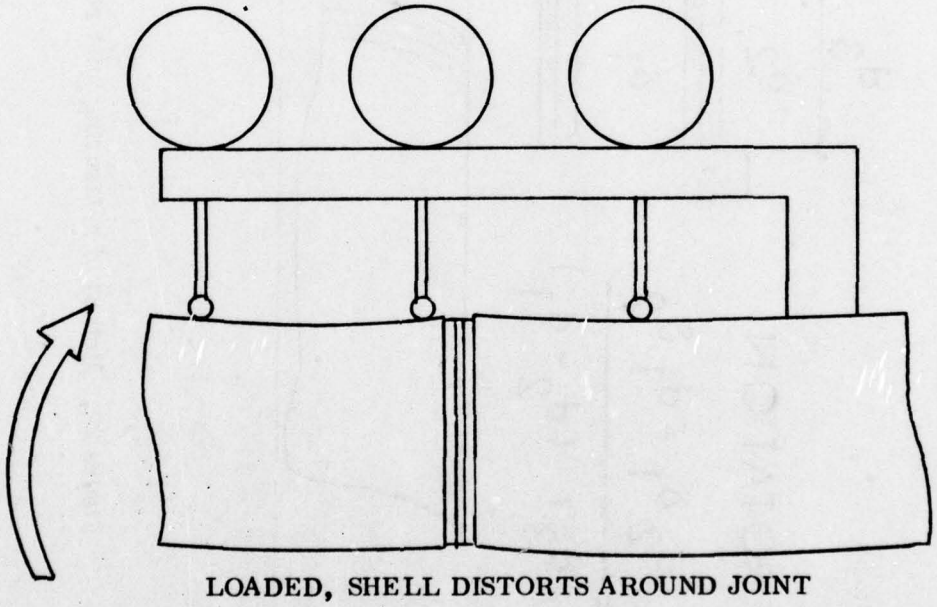

LOADED, SHELL DISTORTS AROUND JOINT

Figure 23. Measurement of joint deflections longitudinally. (Shell distortions due to offset load path through joint cause inaccurate results.)

$$\delta_1 \approx \delta_j + d_1 (\theta_L + \theta_R) \quad \text{(i)}$$

$$\delta_2 \approx \delta_j + d_2 (\theta_L + \theta_R) \quad \text{(ii)}$$

rewrite eq. (ii)

$$(\theta_L + \theta_R) = \frac{\delta_2 - \delta_j}{d_2}$$

substitute into eq. (i)

$$\delta_1 = \delta_j + \frac{d_1}{d_2} (\delta_2 - \delta_j)$$

solving for δ_j:

$$\delta_j \left(1 - \frac{d_1}{d_2}\right) = \delta_1 - \frac{d_1}{d_2} \delta_2$$

$$\delta_j = \frac{d_2 \delta_1 - d_1 \delta_2}{d_2 - d_1}$$

$$\text{joint rotation } (\theta) = \frac{\delta_j}{d_3 r} \text{ rad/in}$$

$$\theta = \frac{d_2 \delta_1 - d_1 \delta_2}{d_3 r (d_2 - d_1)}$$

for the test model

$d_3 = 1.4$ inches
$d_2 = 3.0$ inches
$d_1 = 1.0$ inches
$r = 2.0$ inches

so:

$$\theta_j = \frac{3\delta_1 - \delta_2}{5.6} \quad \frac{\text{radians}}{\text{inch}}$$

The joint specimen was also instrumented with strain gages which served to measure the amount of preload actually obtained and the strains at various critical locations. Figure 24 shows the strain gage placement and grid orientation (axial or tangential). All strain gages were identical; they were Micro-Measurements type CEA-13-062VW-120 having a gage factor of 2.115. They were the single element type, temperature compensated for aluminum. Gage placement was identical on both the tension and compression sides of the joint, all gages were placed in a plane perpendicular to the applied moment.

The gage readings at location B were averaged to obtain the joint preload. The readings at location A were averaged and used as a check to verify the magnitude of the applied moment. All gage readings were compared to NIFDI predictions in order to assess the accuracy of that analytical tool.

5.3 Conventional Joint Tests

Prior to NITINOL preloading the baseline joint was preloaded with torque only and tested. This was done so a direct comparison could be made between performance of the conventional threaded joint and the NITINOL preloaded joint with no other variables present.

5.3.1 Apparatus

The baseline joint specimen was used complete with steel washers and NITINOL ring. It was preloaded with torque only. The NITINOL ring acted only as a spacer in this case and did not serve to preload the joint. Torque was applied using a 0 - 200 foot-pound 'click' type, torque wrench through a special adapter.

For the moment deflection tests, the joint was loaded initially using the hydraulic load cylinder described in Section 5.2.2. It was found that the preload levels obtainable via torque were so low that the resolution

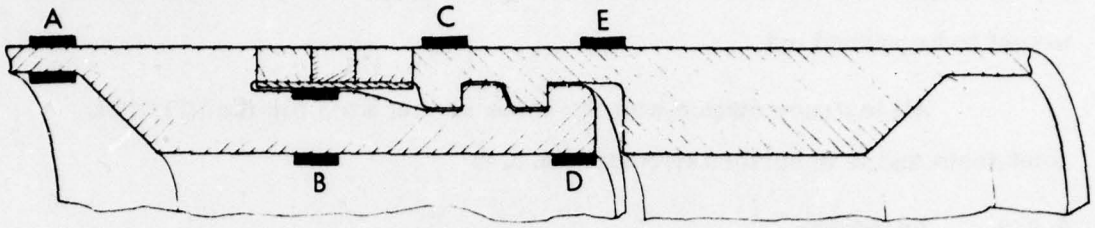

STRAIN GAGES

CEA -13 - 062UW - 120

SINGLE ELEMENT

STRAIN GAUGE NO.	LOCATION	FLEXURE SIDE T-TENSION C-COMPRESSION	ORIENTATION A-AXIAL T-TANGENTIAL
1	A-SHELL O.D.	T	A
2	A-SHELL I.D.	T	A
3	B-THREAD ROOT	T	A
4	B-JOINT I.D.	T	A
5	D	T	T
6	A-SHELL I.D.	C	A
7	A-SHELL O.D.	C	A
8	B-THREAD ROOT	C	A
9	B-JOINT I.D.	C	A
10	D	C	T
11	E	T	A
12	C	T	T
13	E	C	A
14	C	C	T

Figure 24. Strain gage placement. (Placement identical for tension and compression side of joint.)

of the hydraulic cylinder/pressure gage system was inadequate. Therefore, the cylinder was replaced with a spring scale for application of loads in the 0 - 60 pound range (0 - 1440 inch-pounds). A 24 inch moment arm was used for these tests since that was the balance point of the load bar, allowing its weight to be zeroed out.

All instrumentation was the same as that used for the NITINOL joint tests and is described in Section 5.2.3.

5.3.2 Procedure

The test procedure was as follows:

Preparation

1. Attach male side of test joint to load apparatus, and lock in place.
2. Clean and lubricate both male and female threads.
3. Screw joint together, check for interference.
4. Disassemble and visually inspect both halves.
5. Zero all strain gages and record 'zero' reading.
6. Screw joint halves together and torque as required.
7. Record strains, in particular at strain gage location B to determine preload obtained.
8. Attach loading device (spring scale or hydraulic cylinder) and apply load to support weight of load bar.
9. Attach LVDT's and zero; record.
10. Record distance from loading point to joint (moment arm).

Test

1. Apply moments and record LVDT readings; record strain gage output at maximum applied moment.
2. Obtain extra data points in the region where the preload is exceeded.

3. Release load and record all readings.

4. Repeat steps 1 through 3.

5. Torque joint to next value and repeat steps 1 through 4.

5.3.3 Results

The preload obtainable from torque was calculated based on an assumed friction coefficient. The actual preload was measured using the strain gages at location B (Figure 25). The gages were zeroed prior to assembly, after torquing, and the resultant strains were recorded.

The strains were averaged and the preload in meridional pounds per inch was determined. The actual friction coefficients were then calculated using the equation:

$$\mu = \frac{T}{\pi\, pD^2}$$

where T = Torque

μ = friction coefficient

p = preload (meridional pounds/inch)

D = diameter of joint

It was found that the coefficient of friction increased with torque. This trend is one of the factors that limits the amount of torque that can be applied to a threaded joint. Other limiting factors include torsional shell buckling of the thin wall surrounding the joint and localized damage caused to thin wall structures by torque application mehtods.

The joint was initially torqued to 100 foot-pounds. When loaded, the preload was exceeded almost immediately. The apparatus was not set-up to measure the very small moments required so the joint was re-torqued to 200 foot-pounds, and stiffness testing was conducted at that torque level only.

After torquing, LVDT readings and strain gage readings were

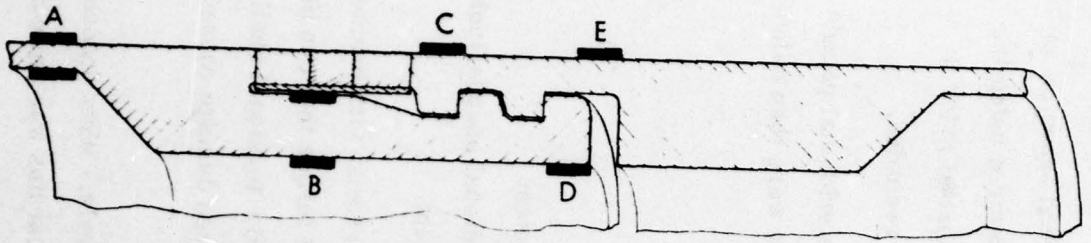

TOTAL CROSS-SECTIONAL AREA AT SECTION B = 1.57 IN^2

Joint Torque ft-lbf	Tension Side Gages B 10^{-6} in. O.D./in. I.D.		Compression Side Gages B 10^{-6} in. O.D./in. I.D.		Average Strain μ in/in	Total Preload (P) (lbs)	Meridional Preload (p) lbs/in.	Coefficient of Friction μ
100	462	-88	590	-243	180	2826	225	0.11
200	810	-190	883	-378	281	4412	351	0.14

Figure 25. Determination of preload torque and effective coefficient of friction.

taken at 480 inch-pound increments (20 pound load increments at 25 inch moment arm). The preload was exceeded at a lower load than predicted. After a load of 9600 inch-pounds had been attained, the load was released, and LVDT readings were taken at 120 inch-pound increments, starting from zero. This time the preload was exceeded at a much lower point than during the first load cycle. Evidently the joint had loosened after the first load cycle. The torque required to disassemble the joint was measured at 40 foot pounds; thus, the torque preloaded joint lost most of its preload after only one load cycle.

The joint was re-torqued to 200 foot-pounds and loads were applied in 120 inch-pound increments. Good definition of the point of preload exceedance was obtained. All data points obtained for that first and second loading cycles of the conventional threaded joint preloaded with torque only appear in Figure 26.

Detailed strain gage readings were taken at a load of 9600 inch-pounds. The resulting stresses, along with those predicted by NIFDI are tabulated in Table 3. The results agree with predictions in direction and roughly in magnitude. It should be noted that at 9600 inch-pounds, the preload of the test joint had been exceeded, whereas the NIFDI predictions were based on a fully preloaded joint.

The point of preload exceedance and apparently the preloaded stiffness were much less than the values predicted. It is hypothesized that this is due to two things: one, 'real' effects, and two, the inability to apply moments to the analytical model.

The analysis assumed all surfaces to be perfectly flat with contact between mating faces (Figure 27a). In reality the mating surfaces are not flat but are covered with machining marks that mesh to form an intermittent point contact pattern. Plane contact does not exist between thread faces; at best, it is line contact (Figure 27b). These effects give rise to additional compliance. Localized yielding at point contact between machining

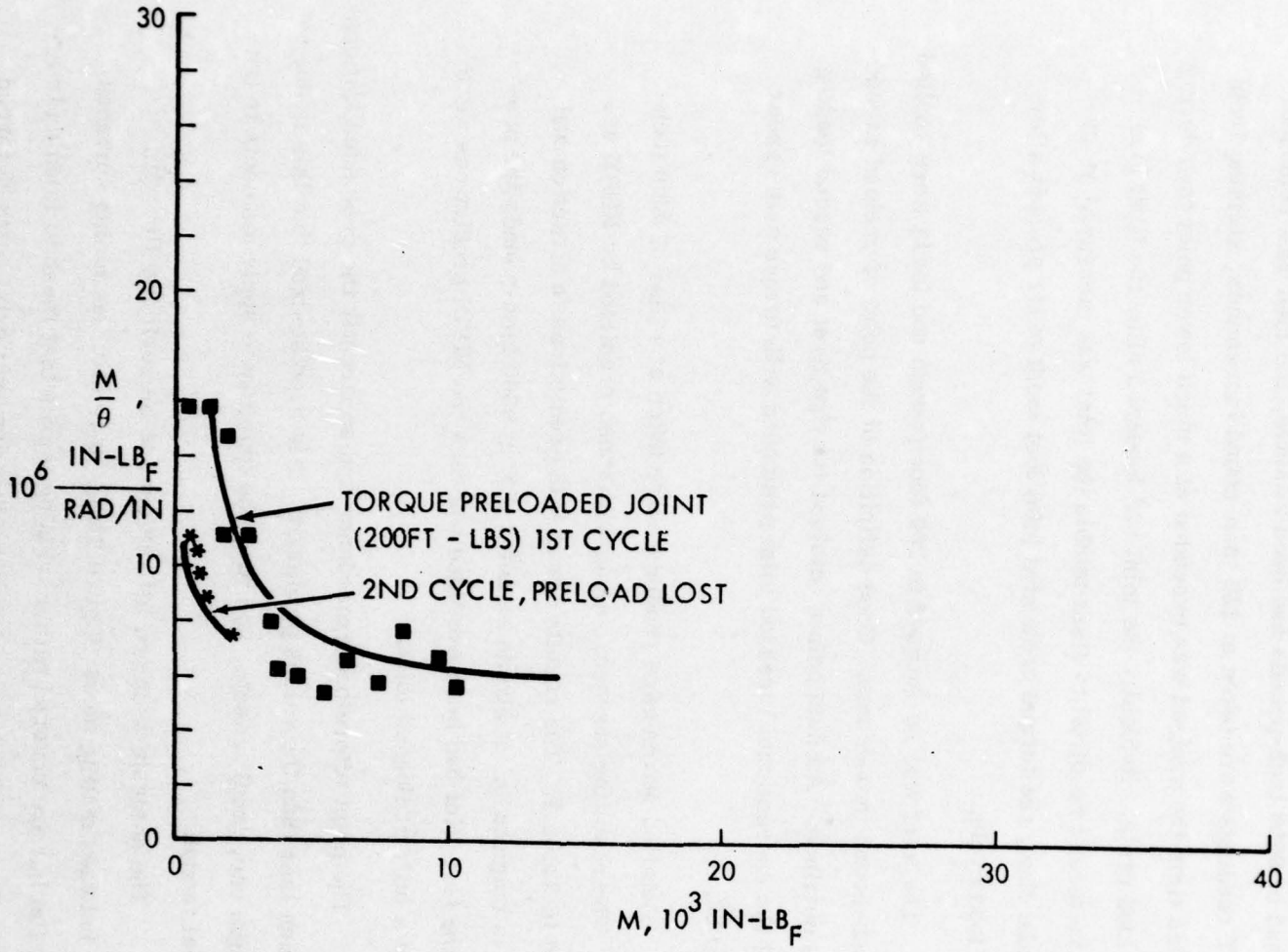

Figure 26. Measured joint stiffness as a function of applied moment, torque preloaded joint.

TABLE 3. SUMMARY OF STRAIN GAGE RESULTS, CONVENTIONAL TORQUE PRELOADED JOINT.

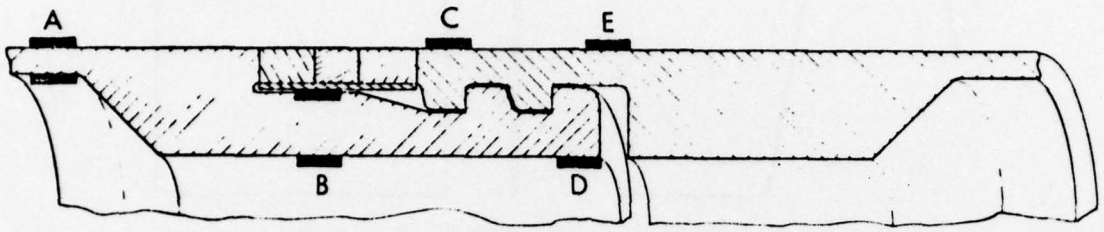

JOINT MOMENT = 9600 INCH-POUNDS

GAGE	A	A	B	B	D	E	A	A	B	B
LOCATION T = TENSION C = COMPRESSION	T	T	T	T	T	C	C	C	C	C
I.D. or O.D.	O.D.	I.D.	O.D.	I.D.	I.D.	O.D.	O.D.	I.D.	O.D.	I.D.
ORIENTATION A - AXIAL T - TANGENTIAL	A	A	A	A	T	A	A	A	A	A
NIFDI ANALYTICAL RESULTS * PRELOADED	14,200	13,040	1,690	-751	-1,895	-5,056	-16,988	-10,480	-2,160	476
EXPERIMENTAL RESULTS * 24-INCH MOMENT ARM	13,310	12,640	8,704	-2,236	-4,370	-6,416	-12,300	-11,800	-3,234	863

(Preload Exceeded)

* Stress in psi.

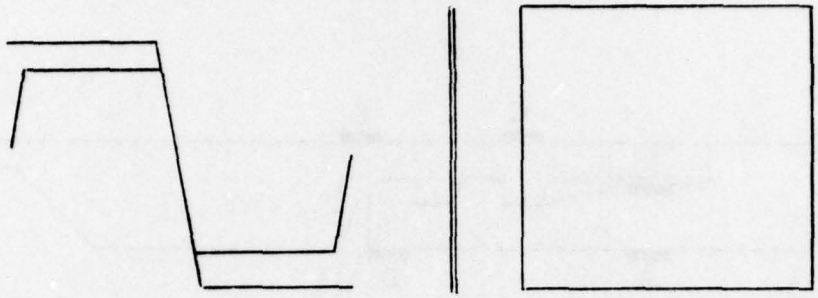

a. Analytical Model, Plane Contact Between Threads, Mating Surfaces are Flat.

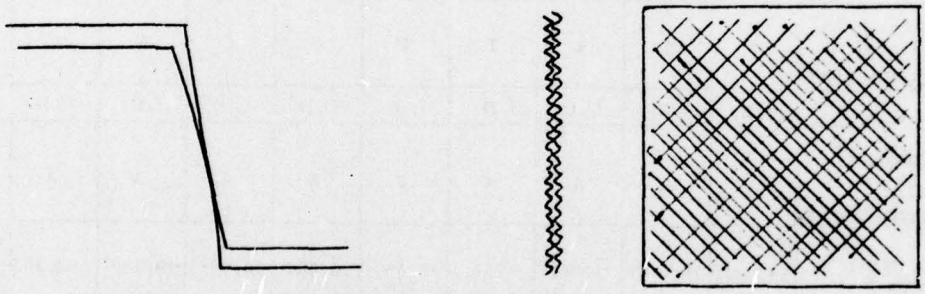

b. Real Joint, Line Contact Between Threads, Machining Marks Produce Pattern of Point Contact Between Mating Surfaces.

Figure 27. Sources of joint compliance.

marks probably resulted in loss of preload after the first cycle.

Moments could not be directly applied to the NIFDI finite element model. So the maximum stresses (tensile and compressive) resulting from the application of a given moment were calculated and converted into tension and compression loads which were applied to the model. Strains resulting from these loads were then used to calculate joint stiffness. The problem with this apprach is that meridional strains are not duplicated (Figure 28), and since meridional strains are a primary source of joint compliance in large diameter, thin wall structures the stiffness predicted by this method is higher than can actually be expected.

5.4 NITINOL Preloaded Joint Tests

A full scale model of the baseline joint was built and tested in order to verify the feasibility of NITINOL preloaded joints and obtain data for comparison to conventional joints.

Techniques were developed that enabled deformation and installation of the NITINOL segment. Stiffness data was measured and compared to that of the conventional threaded joint and NIFDI predictions. Temperature cycling during NITINOL installation failed most of the strain gages; however, they were useful in determining the initial preload obtained.

5.4.1 Apparatus

The joint specimen, load fixture and instrumentation was as described in Section 5.2. Additional appartus required for the NITINOL preloaded joint was as follows:

- 4.5" x 4" I. D. x 0.35" wide aluminum ring (Figure 29). The inside diameter of the aluminum ring was sized so that it had clearance with the steel washers and NITINOL ring at room temperature, but at cryogenic temperatures it contacts on the washers serving two purposes; one, it holds the assembly together for ease of installation and two, it acts as a heat sink

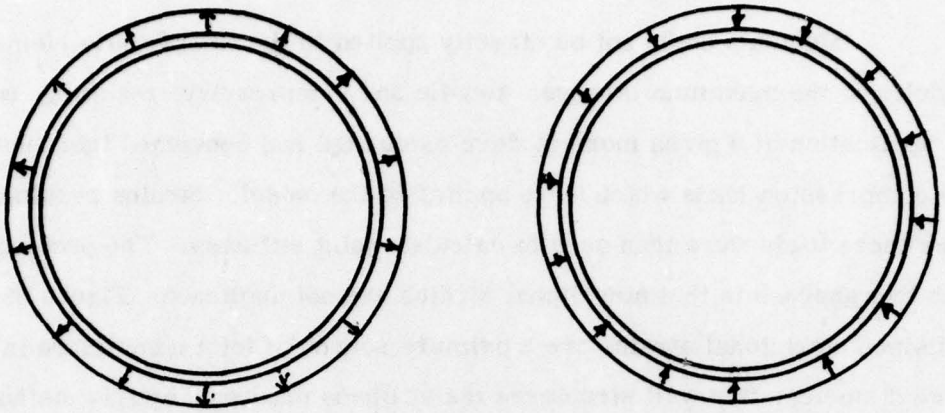

ANALYTICAL MODEL

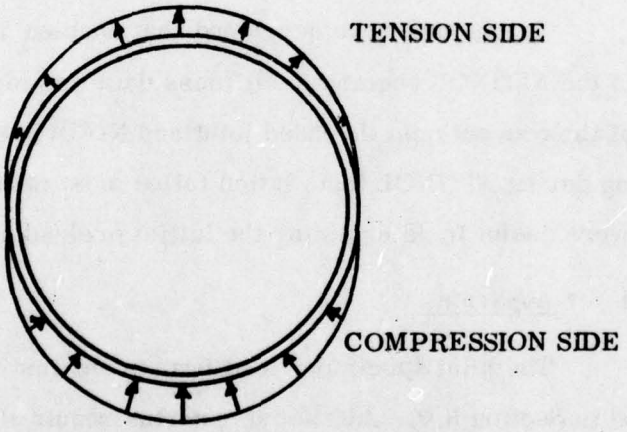

ACTUAL JOINT

Figure 28. Meridional strains due to moment application.

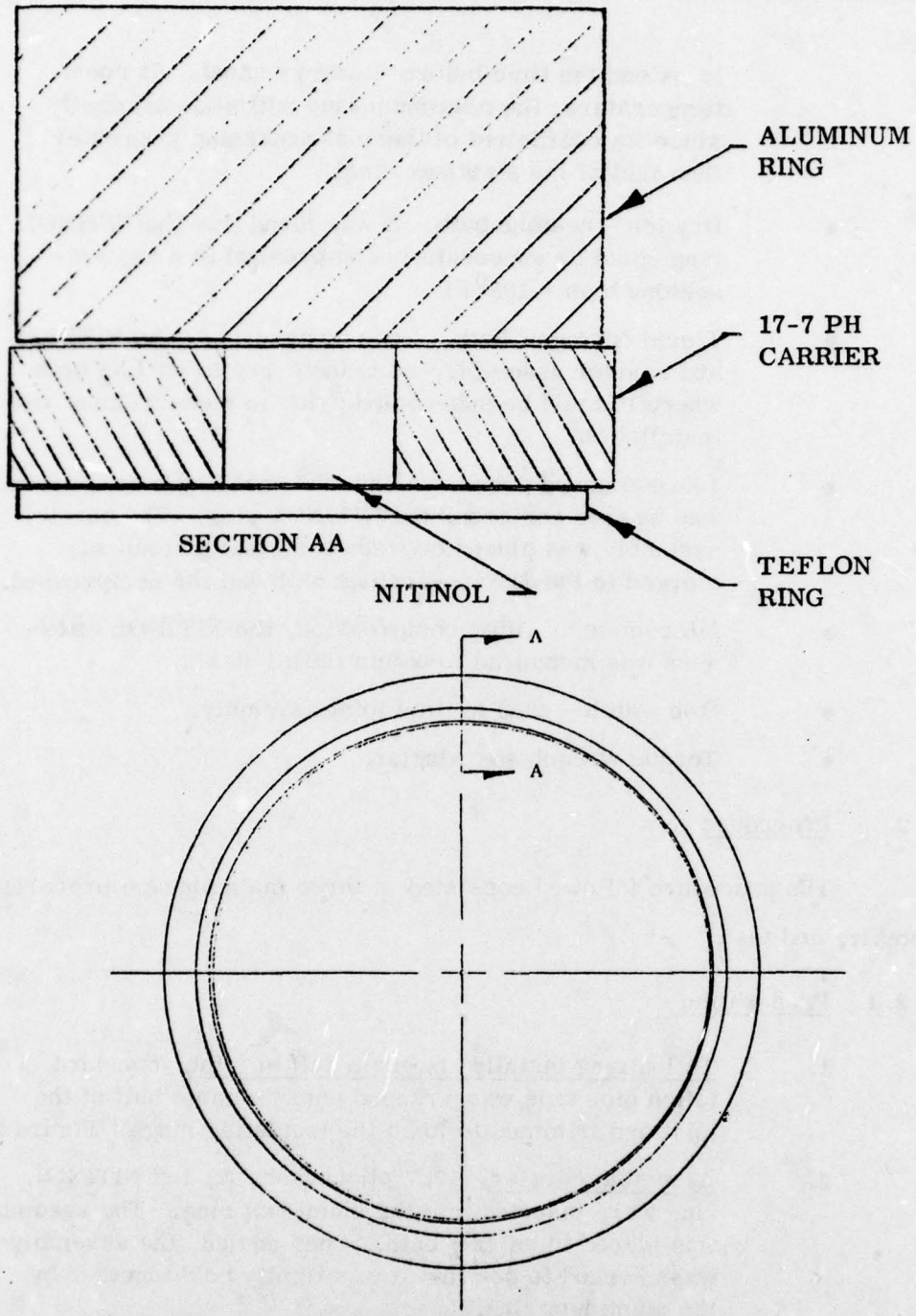

17-7 pH Cover, NITINOL Ring, Aluminum Ring, and Split Teflon Ring as used for NITINOL Installation.

Figure 29. Carrier assembly.

to extend the time before recovery onset. At room temperature, the aluminum ring will slide off easily since its coefficient of thermal expansion is greater than that of the stainless steel.

- Dry ice - acetone bath. It was found that the NITINOL ring could be successfully compressed in a dry ice-acetone bath ($-108^{o}F$).
- Liquid Nitrogen Bath. Once compressed, the NITINOL and carrier assembly was transferred to an LN_2 bath where it could be sub-cooled prior to measurement and installation.
- 100,000 pound press. A 100,000 pound hydraulic press was used to compress the NITINOL ring. The carrier assembly was placed between two steel platens submerged in the dry ice-acetone bath and the compressed.
- Micrometer. After compression, the NITINOL thickness was measured to obtain initial strain.
- Stop watch - used to time joint assembly.
- Torque wrench and adapter.

5.4.2 Procedure

The procedure followed consisted of three main phases: preparation, assembly, and test.

5.4.2.1 Preparation

1. Teflon ring installed on male half of joint. Standard teflon pipe tape was wrapped onto the male half of the joint and trimmed to form the insulating ring of Figure 29.
2. Assemble carrier. 17.7 pH washers (2) and NITINOL ring were inserted into the aluminum ring. The assembly was placed in an LN_2 bath. Once cooled, the assembly was checked to see that it was tightly held together by the aluminum ring.
3. Male half of joint installed on load beam.
4. Fit check. Carrier removed from LN_2 bath, immediately installed in joint and assembled.

5. Practice assembly. Practiced removing the carrier from the LN_2 bath, installing in joint, assembling joint, joint, and torquing. A stop watch was used to measure time from start to finish; practiced until task could be accomplished in less than 15 seconds.

6. Measure NITINOL. Measured thickness of NITINOL ring at several locations and recorded.

7. Compress NITINOL. Placed NITINOL ring between steel platens and submerged in dry ice-acetone bath. Allowed to cool before applying 100,000 pound load.

8. Measure NITINOL. Once compressed, the NITINOL ring was transferred to an LN_2 bath where its thickness was measured.

9. Recovery. Thickness was measured again after NITINOL had recovered at room temperature.

Steps 6-9 were performed to determine how much strain and recovery could be expected from the NITINOL. It was found that approximately 6 percent was obtained.

5.4.2.2 Assembly

1. Chill joint halves. Both the male and female joint halves were chilled prior to assembly to extend the time before the onset of recovery, ensuring that recovery did not begin before the joint was assembled. This was accomplished by insulating around them with foam and packing the inside with dry ice.

2. Assemble Carrier. Assemble the 17-7 pH washers and the NITINOL ring into the aluminum carrier and measure the thickness across both washers and the NITINOL.

3. Chill Carrier. Place the carrier between the two steel platens and place the assembly in the dry ice-acetone bath.

4. Compress. Load the platens with 100,000 pounds. Since the cross-sectional area of the NITINOL is 1.0 square inch, the stress is 100,000 psi.

5. Transfer carrier to LN_2 bath.

6. Measure. Measure across both washers and NITINOL segment while under LN_2 and calculate the amount of strain. Be sure it is at least 5 percent before proceeding.

7. Zero all strain gages on male half of joint.

8. Install. Quickly install carrier onto male half of joint assemble joint and torque to 200 ft-lb. This should be accomplished in 15 seconds or less.

9. Record strain gage readings at location B.

10. Warm joint. Remove insulation and dry ice and warm NITINOL with hair dryer having a maximum temperature of 200° F. (allow 1 - 2 hours)

11. Hook-up strain gages on female half of joint and zero.

12. Install LVDT's and zero

13. Install load bar and hydraulic cylinder.

14. Record strains at location B ; this is an indication of the preload obtained.

5.4.2.3 Test

1. Scribe. Put a scribe line across the joint so it can be observed if the joint loosens.

2. Zero. At zero load zero out all gages and LVDTS; record moment arm of load cylinder.

3. Apply Moment and take LVDT readings at 480 - 2400 inch-pound increments from zero to 28,000 inch-pounds of torque. Take strain gage readings at 3 - 4 points and at maximum load.

4. Release load and record all readings.

5. Repeat steps 2 through 4.

6. Change load cylinder position to vary moment-shear ratio and repeat steps 2 through 5.

5.4.3 Results

Problems associated with building a NITINOL preloaded joint were solved and the baseline joint was successfully assembled. NITINOL preloading produced a significant improvement in joint stiffness over the conventional threaded joint. Joint stiffness (M/Θ) as a function of applied moment (M) was measured from M = 0 to M = 28,000 inch pounds. Good definition of the point of preload exceedance (Mpe) was obtained (21,000 inch-pounds). The results were compared to the conventional threaded joints and NIFDI predictions. Strain gage data was minimal since most failed due to temperature cycling during assembly. Some gages survived long enough to give an indication of the actual preload obtained.

5.4.3.1 NITINOL Implementation

It was originally thought that the NITINOL ring could be deformed at any temperature below its transition temperature; therefore, the plan was to cool the ring with liquid nitrogen (-320°F) prior to deformation. Further, in order to limit the deformation to the recoverable 8 percent, stop blocks were to be used. It was found that satisfactory deformation of the NITINOL ring could not be accomplished at LN_2 temperatures and that stop blocks were not necessary.

The NITINOL ring was cooled to LN_2 temperatures and compressively loaded to 100,000 psi. Measurement of the ring afterwards indicated that no deformation had occurred. A NITINOL sample was cut from the same plate from which the ring was machined. It was cooled in LN_2 and loaded to roughly 200,000 psi at which point it cracked and fractured. Apparently, at -320°F the NITINOL alloy became very strong and brittle. This behavior has been observed for other NITINOL alloys. Figure 30 illustrates stress-strain curves for an alloy having a transition temperature of 75°C. At -196°C (-320°F) its yield point is higher than above its transition temperature.

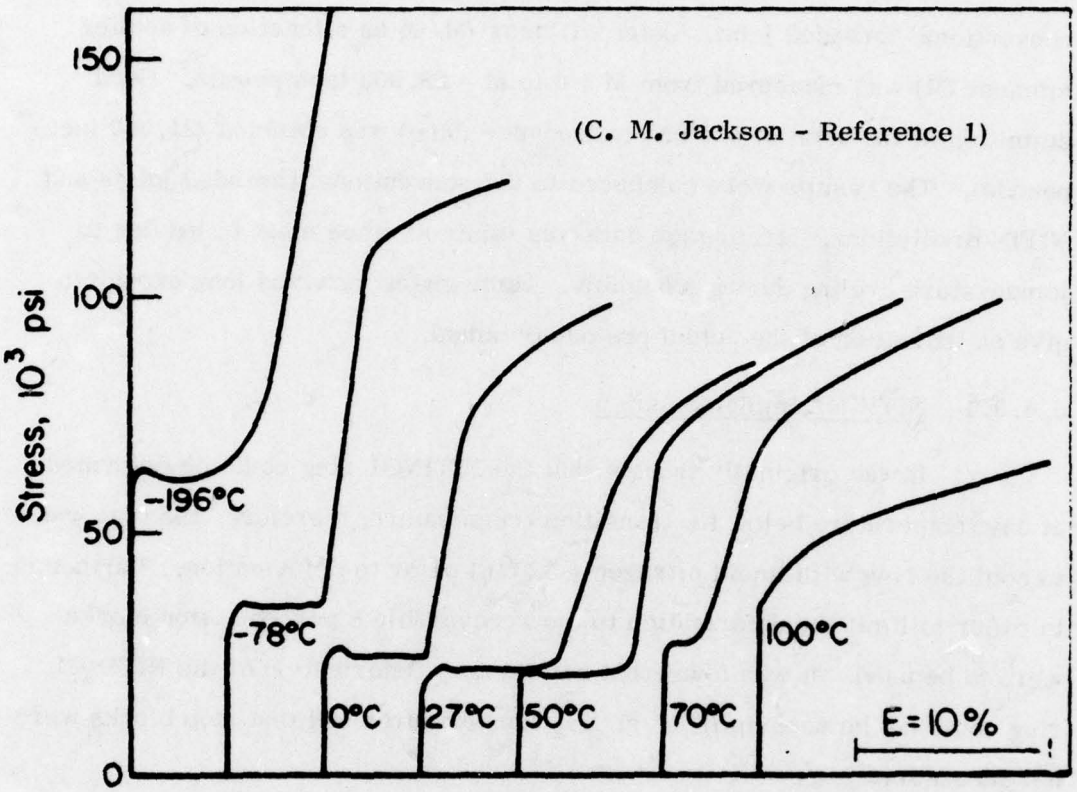

Figure 30. Stress-strain curves for polycrystalline "normalized" NiTi.

(Discontinuous yield and large Luders strains are present below the transformation temperature (75°C.)

The transition temperature of our alloy was reported to be -13°F (-25°C). Deformation was accomplished by placing the NITINOL ring and carrier assembly into a dry-ice acetone bath (-108°F) and immediately applying a load of about 100,000 psi. As the NITINOL cooled to below its transition temperature the load was present and deformation occurred.

Due to the nature of the stress-strain curve of NITINOL below its transition temperature, no stop blocks are necessary. By applying a load in the proper range, deformation is automatically limited to the recoverable 6 - 8 percent. This is because the yield point is low only for a limited amount of deformation, after which it rises sharply. The stress-strain path followed in deforming the NITINOL ring appears in Figure 31.

The thermal insulation system consisting of the two stainless steel washers and the aluminum carrier ring (Figure 29) worked well. After deformation the carrier assembly was sub-cooled in LN_2 before installation in the joint. Both joint halves were cooled to about -40°F prior to assembly. Strain gage readings indicated that NITINOL recovery started about two minutes after installation.

The NITINOL segment was in the form of a continuous ring. It was thought that during compression the diameter might change significantly due to Poisson's effect, and that the ring would have to be segmented to allow installation. This was not the case; after a 6 percent deformation no significant diameter change was measured. The platens evidently offered enough friction to prevent that from happening.

5.4.3.2 Joint Stiffness

The preload obtained with the NITINOL joint was much greater than that of the conventional threaded joint. The high preload had two effects on performance. First, it extended the preloaded stiffness to much higher load levels (from 1200 inch-pounds to 21,000 inch-pounds); and second, the joint did not

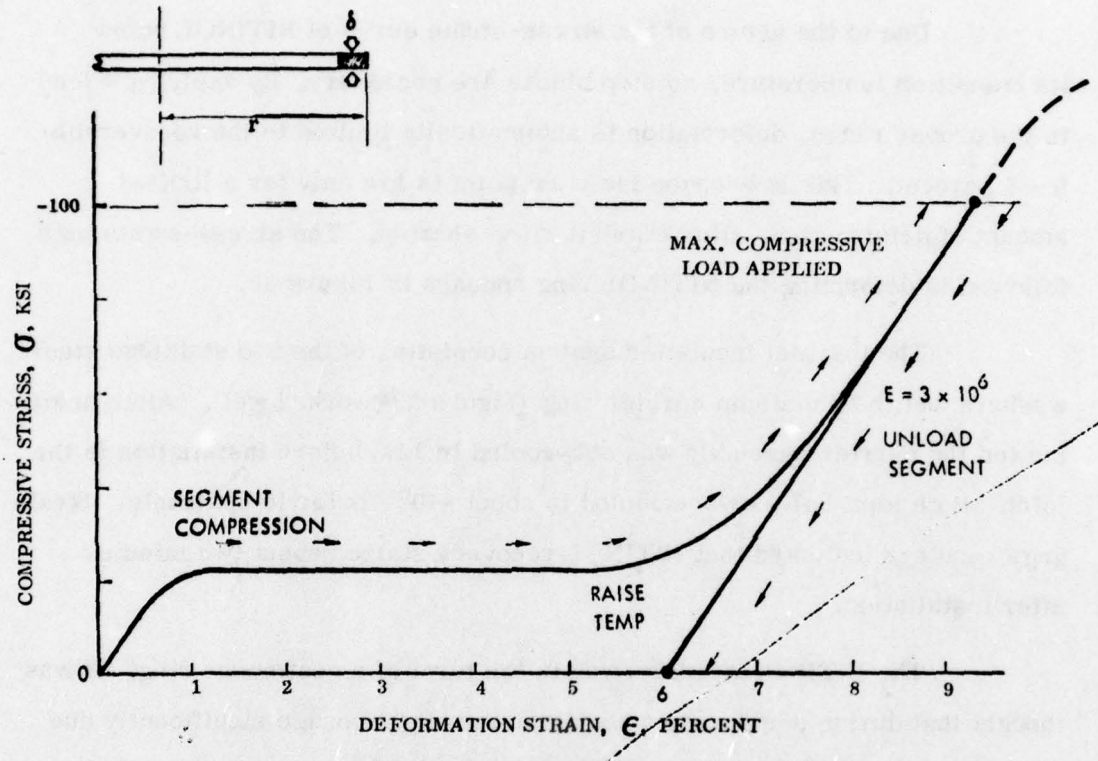

Figure 31. NITINOL stress history.

loosen up during load cycling as was the case for the conventional joint. It would also appear that the preloaded stiffness of the NITINOL joint was approximately 15 percent greater than that of the conventional joint. There were insufficient data points in the preloaded range for the conventional joint to absolutely confirm this, but there is a very good reason why this would be the case. As explained in Section 5.3.3, additional compliance can result from machining marks and inaccurate thread profiles. The NITINOL joint preload was high enough to yield contacting machining marks and thread profiles, thus reducing that source of compliance, which was present for the torque preloaded joint.

Figure 32 is a plot of predicted and measured joint stiffness as a function of applied moment for the NITINOL and conventional joints along with the stiffness of the surrounding shell (no joint structure). The NITINOL joint was loaded to 28,000 inch-pounds on the first load cycle. Subsequent cycles exhibited slightly lower preloaded stiffness. The joint was cycled to 26,000 inch-pounds, a total of 7 times and stiffness did not change after the second cycle. The loss of stiffness after the first cycle was attributed to meridional joint movement after the preload had been exceeded. This movement (Figure 33) was predicted by NIFDI. It resulted in a more compliant load path.

Good definition of the point of preload exceedance (M_{pe}) was obtained. It compares well to the NIFDI predictions since unlike bending, the preload is axisymmetric - as NIFDI modeled it. NIFDI predicted an M_{pe} of 24,000 inch-pounds; 21,000 inch-pounds was measured. The difference is probably because NIFDI predictions were based on 8 percent deformation of the NITINOL segment and only about 6 percent was obtained. NIFDI predicted a preload of 1760 meridional pounds per inch; strain gages indicated that 1516 was obtained. When the predicted M_{pe} is scaled by the actual/theoretical preload the result is an M_{pe} of 20,700; very close to that measured.

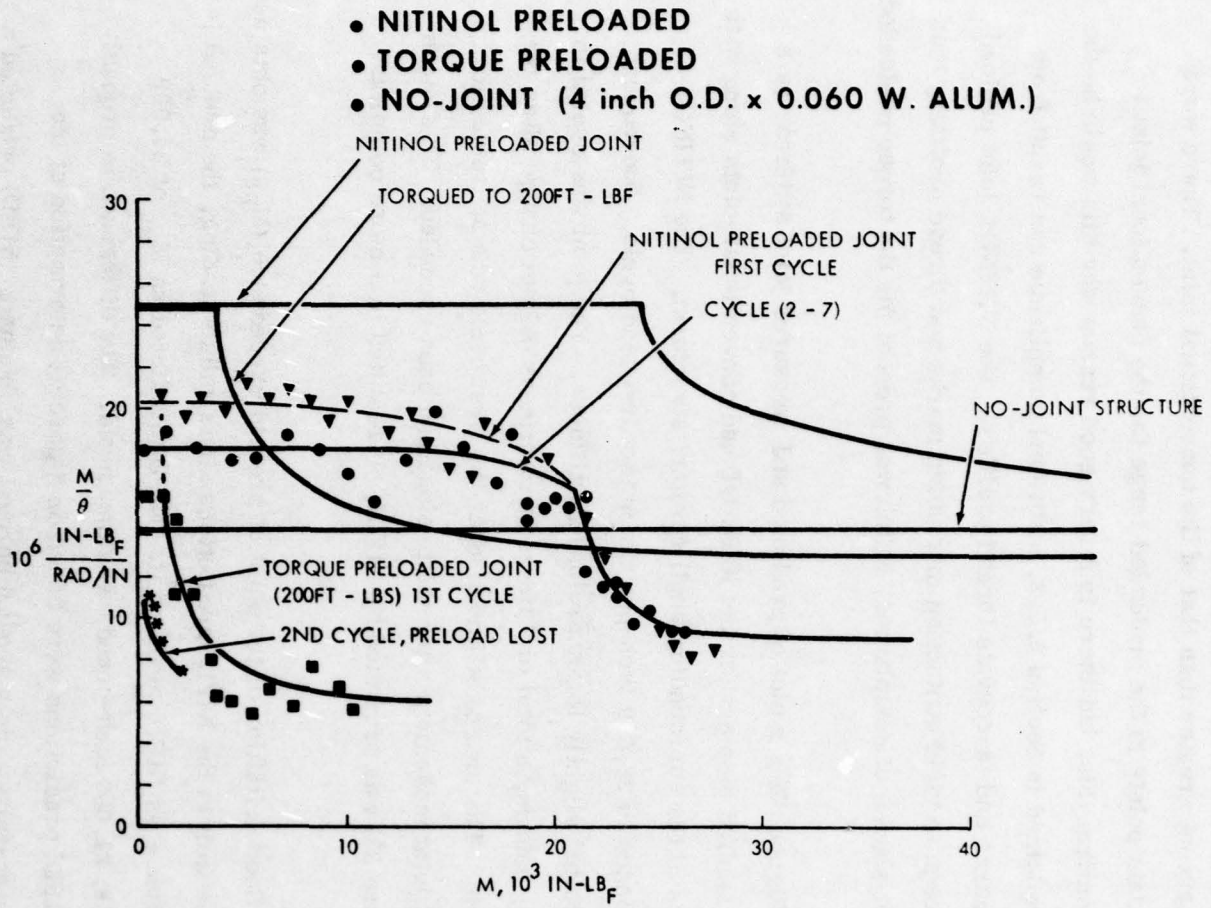

Figure 32. Joint stiffness as a function of applied moment.

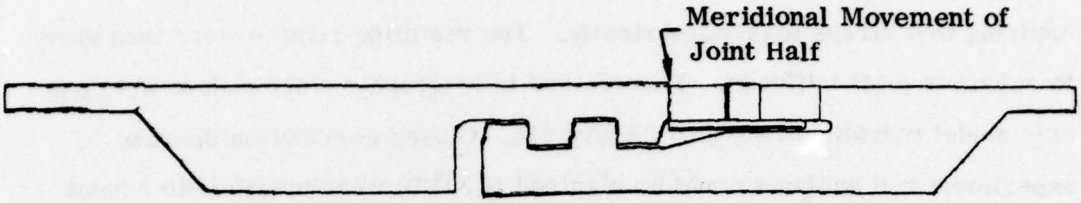

a. NIFDI Predictions

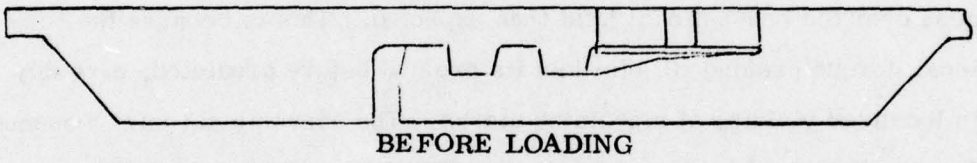

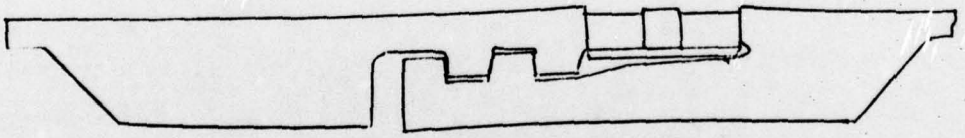

b. Exaggerated Observation

Figure 33. Movement of joint after first load cycle resulted in more compliant load path.

The magnitude of joint stiffness was approximately 30 percent less than predicted by NIFDI. The primary source of this discrepancy is the way moments must be modeled using NIFDI. This was done by calculating the maximum tensile and compressive stresses resulting from a moment and applying that stress axisymmetrically. The resulting strains were then used to calculate joint stiffness. This method is inaccurate since it does not properly model meridional strains (Figure 28). Closer correlation between experiment and analysis could be obtained if NIFDI were modified to accept the application of moments.

Strain gage data was minimal since all but five of the gages failed due to thermal cycling during assembly. A summary of the strain gage results from surviving gages appears in Table 4. The results agreed in direction and roughly in magnitude with NIFDI predictions.

NITINOL preloading produced an even greater improvement in stiffness over the conventional joint than expected. This is because the conventional (torque preloaded) joint lost its preload before predicted, probably due to localized yielding of machining marks. The conventional joint loosened up after the first load cycle, whereas the NITINOL preloaded joint did not.

TABLE 4. SUMMARY OF STRAIN GAGE RESULTS; NITINOL PRELOADED JOINT COMPARISON OF PREDICTED AND MEASURED VALUES FOR ALL SURVIVING STRAIN GAGES.

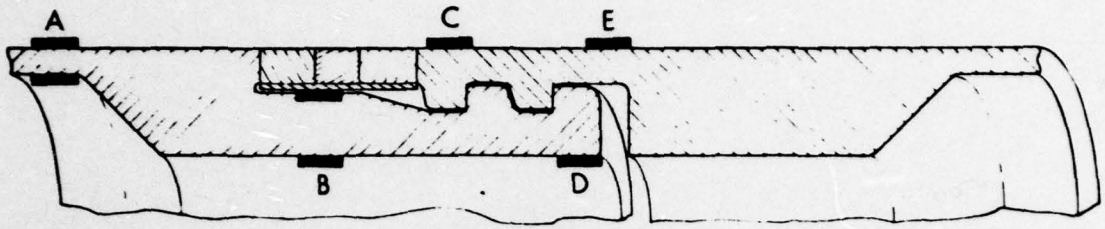

JOINT MOMENT - 20,000 IN-LBF.

	Preload Meridional lbs/in	Gages at A Tension Side Stress (PSI)		Gage at D Tension Side (PSI)	Gage A Compression Side (PSI)	Gage B Compression Side (PSI)
		I.D.	O.D.		O.D.	I.D.
NIFDI ANALYTICAL PREDICTIONS	1,760	27,370	27,167	-3,947	-22,380	922
EXPERIMENTAL RESULTS M/V = 36"	1,516 Measured Via Strain Gage B on Tension Side	27,580	26,630	-550	-25,700	2,600
M/V = 24"		25,388	24,650	---	-23,850	2,548

6.0 CONCLUSIONS

The program demonstrated that NITINOL alloy can be used effectively to preload threaded joints to higher levels than attainable by applying torque. A NITINOL preloaded, threaded joint was successfully designed, analyzed, built, assembled, and tested.

The structural and recovery properties of NITINOL necessary for joint design were determined through a literature search and testing. A NITINOL alloy with a transformation temperature range below the minimum service temperature is most useful for structural applications. Further NITINOL characterization tests are required prior to detailed design of an operational system. Some of the data required for candidate alloys is compressive stress-strain curves both above and below the transition temperature, compressive recovery stress-strain curves, and compressive creep data. The design of joints utilizing NITINOL in tension will require data on bi-axial tension deformation and recovery.

Several joint designs utilizing NITINOL stressed in both tension and compression were conceived. Detailed analyses were performed on a threaded joint preloaded with NITINOL in compression and the same joint preload with torque only. The finite element method was used for analysis; specifically the NIFDI finite element code. The code, equipped with sliding interface elements, proved to be a useful tool for analyzing and designing structural joints with threaded interfaces.

A NITINOL preloaded joint for a baseline 4-inch diameter, 0.060 inch wall, aluminum vehicle was built. Techniques for deformation of the NITINOL segment and assembly of the joint were developed. Development of equipment and procedures for factory or field installations of NITINOL preloaded components is feasible.

A test fixture and instrumentation were developed for the general purpose testing of structural joint stiffness. Both a NITINOL preloaded and conventional torque preloaded joint were tested. Results agreed closely with the NIFDI analyses. NITINOL preloading resulted in a 17-fold increase in the moment causing preload exceedance over the conventional joint. Load cycling did not cause the NITINOL joint to loosen up; it was essentially locked by its high preload; whereas, the conventional, torque preloaded joint loosened up after the first load cycle.

It was determined that the joint preload level greatly affected the design structural weight in cases where the natural frequency of the missile was a limiting design requirement. For the baseline case, a 26 percent reduction in the overall structural weight of the missile could be achieved if NITINOL preloaded joints were used.

The feasibility of utilizing the memory-recovery characteristics of NITINOL to preload structural joints to high levels was successfully demonstrated. Immediate follow-on efforts should be directed towards identifying specific applications and defining their requirements.

7.0 REFERENCES

1. Jackson, C. M., et al, "55-NITINOL--The Alloy with a Memory: Its Physical Metallurgy, Properties, and Applications," prepared by Battelle Memorial Institute for NASA, Report NASA-SP 5110, 1972.
2. Goldstein, David; Naval Surface Weapons Center, "A Source Manual for Information on NITINOL and NiTI," NSWC/WOL TR 78-26, 13 February 1978.
3. Cross, William B., et al, "NITINOL Characterization Study," prepared by Goodyear Aerospace Corporation for Langley Research Center, Report No. NASA CR-1433, September 1969.

APPENDIX

STRUCTURAL TEST DATA

TEST SERIES: NITINOL PRELOADED

MAKE-UP TORQUE: --

MOMENT ARM M/V (INCH): 24

DATE/TIME: 11-11-78

TARE LOAD (V_T) POUNDS: 40

MOMENT: $M = (V - V_T) \frac{M}{V}$

LVDT Gage Factor (G_f) = 100 Volts/Inch

$\delta_1 = -(LVDT1 - LVDT1(TARE))/G_f$

Comments: First Load Cycle

LOAD V POUNDS	LVDT1 (MV)	LVDT2 (MV)
40	428	52
60	401	-14
80	375	-72
100	353	-126
120	330	-179
140	307	-236
160	283	-290
180	259	-351
200	238	-399
200	231	-417
240	189	-518
280	149	-612
320	104	-722
360	58	-834
360	54	-845
400	11	-948
440	-40	-1074
480	-86	-1186
480	-89	-1193
520	-134	-1300
560	-183	-1420
600	-237	-1553
600	-240	-1564
640	-293	-1690
680	-345	-1816
720	-395	-1939
800	-502	-2220
840	-559	-2360
840	-567	-2380

TEST SERIES: NITINOL PRELOADED (Continued)

MAKE-UP TORQUE: --

MOMENT ARM M/V (INCH): 24

DATE/TIME: 11-11-78

TARE LOAD (V_T) POUNDS: 40

MOMENT: $M = (V - V_T) \frac{M}{V}$

LVDT Gage Factor (G_f) = 100 Volts/Inch

$\delta_1 = -(LVDT1 - LVDT1(TARE))/G_f$

Comments: First Load Cycle

LOAD V POUNDS	LVDT1 (MV)	LVDT2 (MV)
880	-617	-2490
920	-676	-2630
920	-685	-2660
960	-738	-2780
1000	-807	-2940
1040	-882	-3110
1080	-960	-3280
1080	-970	-3310
1120	-1052	-3490
1160	-1133	-3670

TEST SERIES: NITINOL PRELOADED

MAKE-UP TORQUE: --

MOMENT ARM M/V (INCH): 36

DATE/TIME: 11-13-78, 1:00

TARE LOAD (V_T) POUNDS: 20

MOMENT: $M = (V - V_T) \frac{M}{V}$

LVDT Gage Factor (G_f) = 100 Volts/Inch

$\delta_1 = -(LVDT1 - LVDT1(TARE))/G_f$

Comments: Second Load Cycle
LVDT's Direct Mounted

LOAD V POUNDS	LVDT1 (MV)	LVDT2 (MV)
20	-71	-20
60	-128	-149
100	-200	-320
140	-273	-494
180	-345	-664
220	-411	-820
260	-488	-1007
300	-570	-1206
340	-655	-1410
380	-729	-1587
420	-793	-1739
460	-865	-1911
500	-941	-2091
540	-1024	-2288
580	-1105	-2480
620	-1199	-2697
660	-1306	-2946
700	-1418	-3202
740	-1535	-3468
500	-947	-2109
520	-979	-2184
540	-1021	-2283
560	-1065	-2389
580	-1107	-2485
600	-1150	-2588
620	-1184	-2665
640	-1234	-2781
660	-1283	-2894
680	-1338	-3018
700	-1390	-3139
720	-1445	-3262

TEST SERIES: NITINOL PRELOADED

MAKE-UP TORQUE: --

MOMENT ARM M/V (INCH): 24

DATE/TIME: 11-13-78, 4:00

TARE LOAD (V_T) POUNDS: 40

MOMENT: $M = (V - V_T) \frac{M}{V}$

LVDT Gage Factor (G_f) = 100 Volts/Inch

$\delta_1 = -(LVDT1 - LVDT1(TARE))/G_f$

Comments: Third Load Cycle

LOAD V POUNDS	LVDT1 (MV)	LVDT2 (MV)
40	-78.6	-17.4
80	-138	-154
120	-186	-265
160	-229	-365
200	-277	-478
240	-320	-578
280	-371	-695
320	-418	-804
360	-465	-913
400	-514	-1026
440	-567	-1148
440	-565	-1146
540	-694	-1445
640	-825	-1750
740	-961	-2100
840	-1099	-2410

TEST SERIES: NITINOL PRELOADED

MAKE-UP TORQUE: --

MOMENT ARM M/V (INCH): 24

DATE/TIME: 11-13-78, 5:00

TARE LOAD (V_T) POUNDS: 40

MOMENT: $M = (V - V_T) \frac{M}{V}$

LVDT Gage Factor (G_f) = 100 Volts/Inch

$\delta_1 = -(LVDT1 - LVDT1(TARE))/G_f$

Comments: Fourth Load Cycle

LOAD V POUNDS	LVDT1 (MV)	LVDT2 (MV)
40	-101	-71
140	-210	-321
240	-315	-568
340	-439	-853
440	-563	-1142
540	-690	-1435
640	-823	-1748
740	-956	-2080
840	-1099	-2410
840	-1083	-2420
940	-1228	-2740
1040	-1406	-3140
1140	-1609	-3580

TEST SERIES: NITINOL PRELOADED

MAKE-UP TORQUE: --

MOMENT ARM M/V (INCH): 24

DATE/TIME: 11-13-78, 5:30

TARE LOAD (V_T) POUNDS: 60

MOMENT: $M = (V - V_T) \frac{M}{V}$

LVDT Gage Factor (G_f) = 100 Volts/Inch

$\delta_1 = -(LVDT1 - LVDT1(TARE))/G_f$

Comments: Fifth Load Cycle, LVDT's Fixed

LOAD V POUNDS	LVDT1 (MV)	LVDT2 (MV)
60	-77	-31
100	-129	-155
140	-170	-253
180	-215	-358
220	-261	-467
260	-310	-582
300	-357	-694
340	-408	-814
380	-451	-919
420	-502	-1042
460	-550	-1154
500	-601	-1282
540	-646	-1389
580	-697	-1511
620	-749	-1633
660	-800	-1757
700	-852	-1881
740	-905	-2005
780	-955	-2124
820	-1008	-2250
860	-1071	-2400
900	-1124	-2525
940	-1181	-2655
980	-1246	-2807
1020	-1315	-2966
1060	-1388	-3131
1100	-1462	-3296

TEST SERIES: NITINOL PRELOADED

MAKE-UP TORQUE: --

MOMENT ARM M/V (INCH): 36

DATE/TIME: 11-13-78

TARE LOAD (V_T) POUNDS: 40

MOMENT: $M = (V - V_T) \frac{M}{V}$

LVDT Gage Factor (G_f) = 100 Volts/Inch

$\delta_1 = -(LVDT1 - LVDT1(TARE))/G_f$

Comments: Sixth Load Cycle

LOAD V POUNDS	LVDT1 (MV)	LVDT2 (MV)
40	-85.4	-77.1
80	-174.2	-282
120	-238	-430
160	-308	-594
200	-379	-757
240	-456	-937
280	-524	-1097
320	-596	-1265
360	-671	-1437
400	-755	-1633
440	-836	-1820
480	-908	-1988
520	-988	-2200
560	-1074	-2400
600	-1175	-2630
640	-1261	-2820

TEST SERIES: NITINOL PRELOADED

MAKE-UP TORQUE: --

MOMENT ARM M/V (INCH): 36

DATE/TIME: 11-13-78, 6:30

TARE LOAD (V_T) POUNDS: 40

MOMENT: $M = (V - V_T) \frac{M}{V}$

LVDT Gage Factor (G_f) = 100 Volts/Inch

$\delta_1 = -(LVDT1 - LVDT1(TARE))/G_f$

Comments: Seventh Load Cycle

LOAD V POUNDS	LVDT1 (MV)	LVDT2 (MV)
40	-64	-002
80	-159	-226
120	-226	-386
160	-295	-548
200	-370	-723
240	-452	-920
280	-527	-1100
320	-599	-1274
360	-670	-1445
400	-744	-1622
440	-821	-1809

TEST SERIES: TORQUE PRELOADED

MAKE-UP TORQUE: 200 ft-lbf

MOMENT ARM M/V (INCH): 24

DATE/TIME: 11-9-78, 4:00

TARE LOAD (V_T) POUNDS: 20

MOMENT: $M = (V - V_T) \frac{M}{V}$

LVDT Gage Factor (G_f) = 100 Volts/Inch

$\delta_1 = -(LVDT1 - LVDT1(TARE))/G_f$

Comments: First Load Cycle

LOAD V POUNDS	LVDT1 (MV)	LVDT2 (MV)
20	7.9	14.4
40	-4.4	-15
63	-29.4	-74.0
80	-56.4	-136
100	-94.2	-221
120	-126.8	-295
140	-183	-434
160	-208	-477
180	-260	-590
220	-369	-831
260	-492	-1104
300	-588	-1316
340	-705	-1577
380	-783	-1748
420	-883	-1966

TEST SERIES: TORQUE PRELOAD ONLY

MAKE-UP TORQUE: 200 ft-lbf

MOMENT ARM M/V (INCH): 24

DATE/TIME: 11-10-78, 2:00

TARE LOAD (V_T) POUNDS: 37

MOMENT: $M = (V - V_T)\ \frac{M}{V}$

LVDT Gage Factor (G_f) = 100 Volts/Inch

$\delta_1 = -(LVDT1 - LVDT1(TARE))/G_f$

Comments: First Load Cycle
(After Re-torqueing)

LOAD V POUNDS	LVDT1 (MV)	LVDT2 (MV)
37	-65.1	-47.2
45	-74.8	-69.8
49.5	-80.1	-82.2
54	-85.7	-95.3
60	-93.6	-113.3
65	-100.6	-129.3
70	-107.1	-144.5
75	-114.2	-160.9
80	-121.1	-177.2

TEST SERIES: TORQUE PRELOAD ONLY

MAKE-UP TORQUE: 200 ft-lbf

MOMENT ARM M/V (INCH): 24

DATE/TIME: 11-10-78, 12:00

TARE LOAD (V_T) POUNDS: 40

MOMENT: $M = (V - V_T) \frac{M}{V}$

LVDT Gage Factor (G_f) = 100 Volts/Inch

$\delta_1 = -(LVDT1 - LVDT1(TARE))/G_f$

Comments: Second Load Cycle

LOAD V POUNDS	LVDT1 (MV)	LVDT2 (MV)
40	-5.4	-28.7
45	-17.8	-57.2
50	-29.2	-83.8
55	-38.5	-105.6
60	-49.5	-130.9
65	-57.3	-148.5
70	-69.2	-176.0
75	-77.5	-195.0

DISTRIBUTION LIST

	Copies
Navy	
Naval Surface Weapons Center White Oak Laboratory Silver Spring, Maryland 20910	
G-40	1
G-402 (Huang)	5
G-41	1
G-402 (Matra	9
K-82 (Edwards)	1
WX-21	13
WS-10 (Reinhard)	1
Naval Surface Weapons Center Dahlgren Laboratory Dahlgren, Virginia 22448	
CG (Soper)	1
Office of Chief of Naval Operations Operations Evaluation Group (OP-03EG) Washington, D. C. 20350	1
Defense Nuclear Agency Washington, D. C. 20301	2
Commander Naval Sea Systems Command Washington, D. C. 20360	
Code SEA-03A	1
Code SEA-0333	1
Code SEA-035	2
Code SEA-035A	1
Code SEA-55212	1
Code SEA-0632	2
Commander Naval Air Systems Command (AIR-320-B) Washington, D. C. 20360	1
Commander Naval Missile Center Point Mugu, California 93041	
Mr. T. W. Elliott (Code 5331)	1

	Copies
Commander Naval Air Development Center Johnsville, Warminster, Pennsylvania 18974	
Dr. E. McQuillan (Code 3033)	1
Commander Naval Research Laboratory Washington, D. C. 20390	
Dr. M. R. Achter (Code 6340)	1
Commander Naval Weapons Center China Lake, California 93557	
Code 4062	1
Code 45703	1
Mr. E. L. Jeter	1
Chief of Naval Research Washington, D. C. 20360	
Code 461	1
Code 439 IN. Perrone	1
Code 470	1
Technical Library	2
Naval Postgraduate School Monterey, California 93940	
Code 2124	1
Dr. J. G. Cantin	1
Commanding Officer Naval Ship Research and Development Center Bethesda, Maryland 20034	
Code 1884 (J. McKee)	1
Code 1884 (G. Everstine)	1
Code 564	2
Air Force	
AFFDL/PTS (Capt. G. L. Camburn) AF Flight Dynamics Laboratory Wright-Patterson Air Force Base, Ohio 45433	1
AF Materials Laboratory Wright-Patterson Air Force Base, Ohio 45433	
Code MAAN (B. R. Emrich)	1

	Copies
Flight Dynamics Laboratory Structures Division Wright-Patterson Air Force Base, Ohio 45433 Mr. Leo J. D. Bernier	1
AFML/LLM (W. G. Ramke) Wright-Patterson Air Force Base, Ohio 45433	1
AFATL/DLRV Eglin Air Force Base, Florida 32542 Mr. J. M. Heard	2
Army	
Commanding General U.S. Army Missile Command Redstone Arsenal, Alabama 35809	1
Other Agencies	
NASA Scientific and Technical Information Facility P. O. Box 33 College Park, Maryland 20740 Acquisition Branch - Foreign Exchange	2
TOTAL	71